Copyright Warning & Restrictions

The copyright law of the United States (Title 17, United States Code) governs the making of photocopies or other reproductions of copyrighted material.

Under certain conditions specified in the law, libraries and archives are authorized to furnish a photocopy or other reproduction. One of these specified conditions is that the photocopy or reproduction is not to be "used for any purpose other than private study, scholarship, or research." If a, user makes a request for, or later uses, a photocopy or reproduction for purposes in excess of "fair use" that user may be liable for copyright infringement,

This institution reserves the right to refuse to accept a copying order if, in its judgment, fulfillment of the order would involve violation of copyright law.

Please Note: The author retains the copyright while the New Jersey Institute of Technology reserves the right to distribute this thesis or dissertation

Printing note: If you do not wish to print this page, then select "Pages from: first page # to: last page #" on the print dialog screen

-ABSTRACT

ELECTRICAL, ELECTRONIC and OPTICAL PROPERTIES OF MoS_2 & WS_2

by
Weitao Tang

Two dimensional materials such as graphene, boron nitride and transition metal dichalcogenide (TMDCs) monolayers have arisen as a new class of materials with unique properties at monolayer thickness. Their electrical, electronic and optical properties are of great importance for a variety of applications in optoelectronics as light emitters, detectors, and photovoltaic devices. This work focuses on MoS_2 and WS_2, which are two important members of the TMDC class of materials. The properties of monolayer MoS_2 and WS_2 are investigated as well as the properties of bulk MoS_2 and WS_2 to provide an understanding of their significant difference.

A detailed investigation of the electrical and electronic properties including temperature dependent resistivity, contact resistance, band structure and electronic excitation are discussed in this work. The temperature dependence of the energy gap for monolayer MoS_2 and WS_2 is also investigated. The optical properties of MoS_2 and WS_2, in the range of 1.5-3.0 eV, are modeled utilizing MATLAB simulations. Simulations of the optical properties of these materials on silicon, gold and fused silica substrates are presented. The optical band gap is simulated in order to compare with the electrical band gap. The future applications of both the materials are discussed.

ELECTRICAL, ELECTRONIC and OPTICAL PROPERTIES OF MoS_2 & WS_2

by
Weitao Tang

A Thesis
Submitted to the Faculty of
New Jersey Institute of Technology
in Partial Fulfillment of the Requirements for the Degree of
Master of Science in Materials Science and Engineering

Interdisciplinary Program in Materials Science and Engineering

January 2017

APPROVAL PAGE

ELECTRICAL, ELECTRONIC and OPTICAL PROPERTIES OF MoS_2 & WS_2

Weitao Tang

Dr. Nuggehalli M. Ravindra, Thesis Advisor — Date
Professor, Department of Physics, NJIT

Dr. Yuanwei Zhang, Committee Member — Date
Assistant Professor, Department of Chemistry and Environmental Science, NJIT

Dr. Michael Jaffe, Committee Member — Date
Research Professor, Department of Biomedical Engineering, NJIT

BIOGRAPHICAL SKETCH

Author: Weitao Tang

Degree: Master of Science

Date: January 2017

Undergraduate and Graduate Education:

- Master of Science in Materials Science and Engineering,
  New Jersey Institute of Technology, Newark, NJ, 2016

- Bachelor of Science in Material Chemistry,
  Tianjin University, Tianjin, P. R. China, 2014

Major: Materials Science and Engineering

Publications:

Sushant S. Rassay, Weitao Tang, Nuggehalli M. Ravindra
"OPTICAL PROPERTIES AND TEMPERATURE DEPENDENCE OF ENERGY GAP OF TRANSITION-METAL DICHALCOGENIDES"
Proceedings Materials Science & Technology (MS&T) 2016, Salt Lake City, Utah, October 23-27 (2016).

"To my parents who keep supporting and encouraging me all these years and never give up the immature me."

ACKNOWLEDGMENT

I would like to express my sincere appreciation to my thesis advisor and academic advisor Dr. N. M. Ravindra for his unwavering guidance, encouragement and patience. Without his knowledge and help, this work would not have been possible.

I would also like to express my appreciation to Dr. Yuanwei Zhang and Dr. Michael Jaffe for serving as members of my thesis committee.

I should add that my colleague, Sushant Rassay, has collaborated with me and provided me with the essential materials and advice for the entire year. I also received technical support from my friend, Keyuan Wu in MATLAB. I would like to express my appreciation for help and encouragement that I received from both of them and also their helpful spirits that supported me.

I would like to express my sincere appreciation to my parents for providing selfless mental guidance and economic support for the past 24 years.

TABLE OF CONTENTS

TABLE OF CONTENTS
(Continued)

Chapter **Page**

LIST OF TABLES

LIST OF FIGURES

LIST OF FIGURES
(Continued)

Figure **Page**

CHAPTER 1

INTRODUCTION

1.1 Introduction

Two-dimensional materials such as graphene, boron nitride and transition metal dichalcogenide (TMDCs) monolayers have drawn enormous interest in materials science because of their distinctive properties at monolayer thickness. This work focuses on MoS_2 and WS_2, which are two important members of the TMDC class of materials. Their electrical, electronic and optical properties are promising for a variety of applications in optoelectronics as light emitters, detectors, and photovoltaic devices. The properties of monolayer MoS_2 and WS_2 are investigated as well as the properties of bulk MoS_2 and WS_2 to give a better understanding of their significant difference.

In the first part of this study, a brief introduction to the molecular structure of the two materials is presented in Section 1.2. In Chapter 2, the electrical properties of the two materials are discussed including the temperature dependent resistivity and contact resistance. In Chapter 3, their electronic properties such as band structure, electronic excitation and temperature dependence of the band gap are investigated. The optical properties including dielectric constants, complex reflective index, optical band gap and spectral properties are investigated in Chapter 4 utilizing MATLAB simulations. Also, the spectral properties of monolayer MoS_2 and WS_2 on silicon, gold and fused silica are investigated to promote future applications in optical and optoelectronic devices. Chapter 5 presents a general conclusion of this study and provides some recommendations for future directions.

1.2 Overview of MoS_2 &WS_2

The layered transition metal dichalcogenides (TMDCs) i.e. MX_2 are typical 2D semiconductors with atomic scale thickness. M refers to a transition metal atom such as Mo, W, etc. while X refers to a chalcogen atom. Monolayer TMDCs present distinctive properties from bulk TMDCs and thus draw enormous interest.

The TMDC monolayers are direct band gap semiconductors while bulk TMDCs are indirect band gap with a smaller band gap. The lack of inversion center also allows high degree of freedom for charge carriers or k-valley index and thus lead to valleytronics [1]. In bulk TMDCs, the TMDC layers are combined with each other, layer by layer, with Van-der-Waals force, and the week interaction between layers greatly influences the properties of the bulk TMDCs. TMDCs can also combine with other 2D materials to form Van-der-Waals heterostructure devices through week Van-der-Waals force[2].

1.2.1 Monolayer Structure

The bulk TMDCs are stacked by monolayer TMDCs through Van-der-Waals force. Thus, in order to understand the structure of bulk TMDCs, the structure of monolayer TMDCs need to be studied first.

As shown in Figure1.1, the monolayer TMDCs have interior layered structure. One layer of transition metal atoms is sandwiched between two layers of chalcogen atoms. The bonds between the transition metal atom and transition metal atom, chalcogen atoms and chalcogen atoms, transition metal atoms and chalcogen atoms are all covalent bond, and thus, much more stable compared with the week Van-der-Waals force between bulk layer.

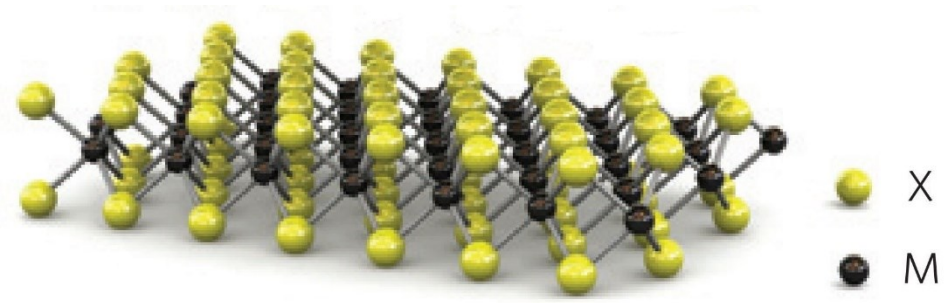

Figure 1.1 Structure of monolayer TMDCs; M represents transition metal atoms while X stands for chalcogen atoms [3].

Both the MoS_2 monolayer and WS_2 monolayer have a thickness of 0.65nm[4]. The ultrathin thickness of the two materials enables more light to pass through the structure and thus reduces the optical absorptance. Unlike the most commonly studied 2D material: graphene, these materials have intrinsic direct band gap, and thus are promising in fabricating new transistor channel as an ideal switch material[5]. It should be noted that the direct band structure of both the materials are sensitive to strain[6, 7]. The direct band structure in WS_2 can be transformed to indirect band gap with only 1% strain[7]. The electronic properties of these materials will be further discussed in Chapter 2.

1.2.2 Bulk Structure

Bulk MoS_2 and Bulk WS_2 are both inorganic compounds. They are all classified as metal dichalcogenides and have similar structure.

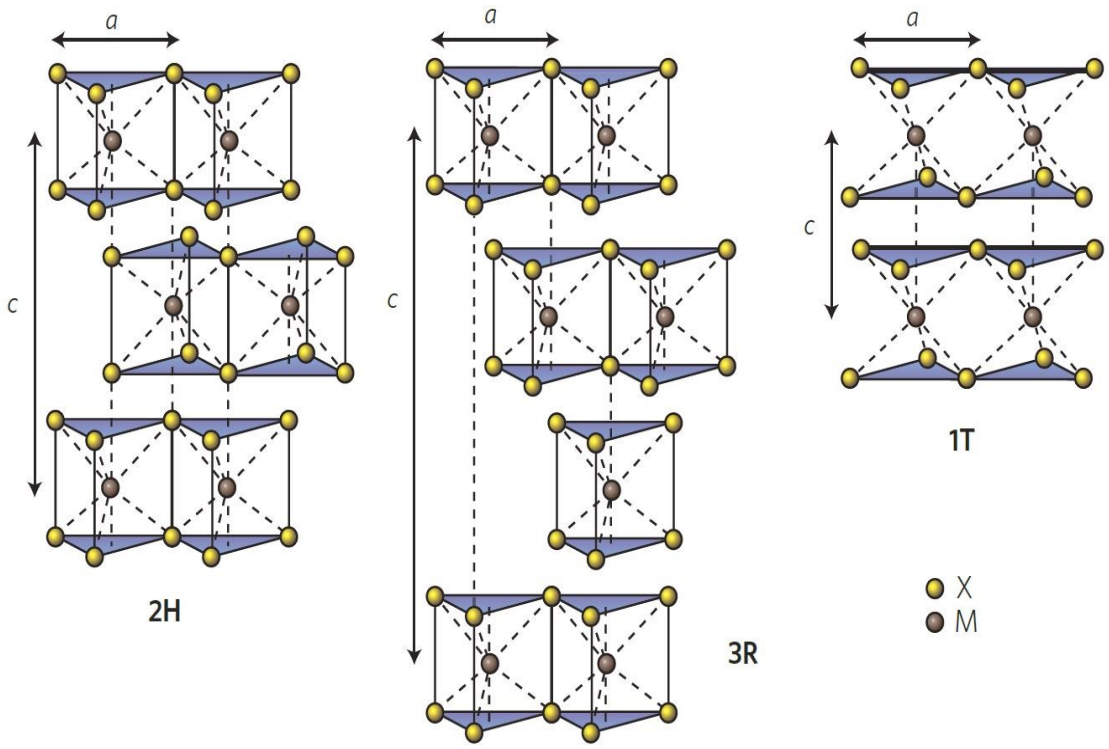

Figure 1.2 Structure of bulk TMDCs; M represents transition metal atoms while X stands for chalcogen atoms [3].

Figure 1.2 presents the structure of bulk TMDCs, which includes MoS_2 and WS_2. Bulk TMDCs contain three types of structure: 1T, 2H and 3R. The three structures represents different combination of single layers by week Van-der-Waals force. It should be noted that bulk TMDCs often consist of all these three structures, and is not formed by only one of the structures. The 2H structure is the most abundant structure in the bulk crystal[8]. In the 2H structure, the metal atoms stay in the center of a trigonal prismatic coordination sphere which consists of one metal atom and six chalcogen atoms, and each chalcogen atom is bonded with three metal atoms. Because each layer is combined by week Van-der-Waals force, bulk TMDCs can be exfoliated to form single or few layer structure/s.

Table 1.1 Physical Properties of Bulk MoS_2 and WS_2

	Molybdenum disulfide	Tungsten disulfide
Chemical formula	MoS_2	WS_2
Molar Mass	160.07 g/mole [9]	247.98 g/mole [9]
Density	5.06/cm^3 [9]	7.5 g/cm^3 [9]
Melting point	1,185 °C decompose	1250°C decompose
Crystal structure	hP6, space group P6 3/mmc, No 194 (2H) hR9, space group R3m, No 160 (3R)	
Lattice constants	a = 0.3160nm, c/a= 3.89 (2H) [10]	3.154nm, c/a=3.920 (2H) [10]
Solubility	Insoluble in water [9]	Slightly soluble in water [9]

Table 1.1 presents the physical properties of bulk MoS_2 and WS_2. Bulk MoS_2 crystal is a silvery black solid and bulk WS_2 crystal is dark gray. They both present dry lubricant properties. The monolayer TMDCs can be produced from the bulk crystal by chemical vapor deposition, liquid exfoliation and mechanical exfoliation; the last method provides much cleaner, more pristine and higher quality structures, which are more suitable for fundamental studies and potential applications[6].

CHAPTER 2

ELECTRICAL PROPERTIES OF MoS_2 & WS_2

In Chapter 1, a succinct introduction to the structures of the monolayer and bulk MoS_2 and WS_2 are provided. In this chapter, a literature review of the electrical properties of MoS_2 and WS_2 are presented. The temperature dependence of electrical properties such as sheet conductivity and field effect mobility are discussed to study the conduction mechanism in order to understand the performance of electrical devices by MoS_2 and WS_2 monolayers.

2.1 Background Knowledge

2.1.1 Hall Effect

Hall effect is the most common method used to characterize the electrical properties of conductors and semiconductors. It is a simple, low cost and time saving method that is used to characterize the carrier concentration, conductivity, resistivity and the mobility, as function of temperature, in industry or laboratories. Thus, it is necessary to give an introduction to Hall effect for a better understanding of the experimental results.

Hall effect is due to the nature of the current in a conductor. Figure 2.1 presents an illustration of the Hall effect. Current is the flow of charge carriers in the conductor. These charge carriers can be electrons, holes and ions. When there is a voltage drop applied across a material, the electrical field created by the voltage drop applies electrical forces to the free carriers inside the material, and thus, the carriers move at certain direction depending on the direction of the electric field and the charge type of the carriers. It is obvious that all the electrical properties are fundamentally the properties of the charge carriers. When a

magnetic field is applied vertically to the current, the magnetic field will apply a force to the moving carriers due to electromagnetic induction, and this force is called Lorentz force.

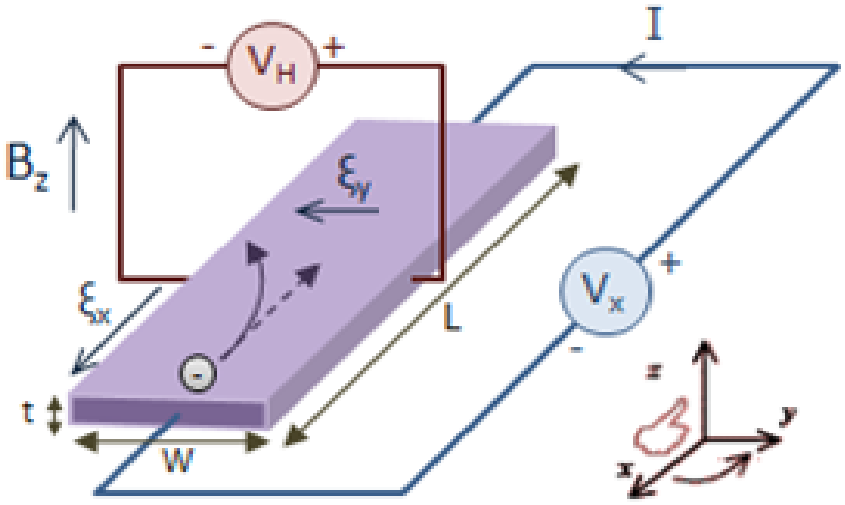

Figure 2.1 Illustration of Hall effect.

source: https://en.wikipedia.org/wiki/Hall_effect

The direction of force is vertical to the direction of carrier flow following Maxwell equations. This results in carriers that are generated at the boundary of the material. This also leaves equal and opposite charges exposed on the other side of the boundary due to lack of charge carriers. The asymmetric distribution will generate another voltage drop and applies another electric force to the moving carriers and the direction of the force will be opposite to the direction of the Lorentz force. The carriers generated at the boundary will increase with time; also, the electric field due to the opposite carriers at the boundary and electric force applied to the moving carriers will both increase. At certain times, the electric force by the opposite charge on both sides of the boundary will neutralize the Lorentz force induced by the magnetic field, and the moving carriers will be able to move in the original

direction regardless of the former two forces. If we measure the current and the voltage in the flow direction as well as vertical to the flow, we can calculate the corresponding electrical properties of the material with the following equations.

For a certain carrier in a material, there are two forces in the y direction; one is the electrical force by the opposite charge on both sides of the boundary, while the other is the Lorentz force by the magnetic field. The total force is given by Equation 2.1:

$$\boldsymbol{F} = q^*[\,\boldsymbol{E} + (\,\boldsymbol{v} \times \boldsymbol{B}\,)] \tag{2.1}$$

As mentioned above, the total force in the y direction should be zero to ensure that the carriers do not move in the y direction. This leads to Equation 2.2:

$$0 = \boldsymbol{E}_{\mathbf{y}} - \boldsymbol{v}_{\mathbf{x}} \times \boldsymbol{B}_{\mathbf{z}} \tag{2.2}$$

The electric field in the y direction is generated by the voltage in the y direction as given by Equation 2.3:

$$\boldsymbol{E}_y = \frac{\boldsymbol{V}_H}{\boldsymbol{w}} \tag{2.3}$$

Combing Equations 2.2 and 2.3 leads to Equation 2.4:

$$\boldsymbol{V}_{\mathrm{H}} = \boldsymbol{v}_{\mathrm{x}} \times \boldsymbol{B}_{\mathrm{x}} * \boldsymbol{w} \tag{2.4}$$

For the electron current, we have Equation 2.5 where n is the current density:

$$\boldsymbol{I}_x = \boldsymbol{ntw}\,(-\boldsymbol{v}_x)(\boldsymbol{-e}) \tag{2.5}$$

Combing Equations 2.4 and 2.5 to exclude **w**, Equation 2.6 is:

$$\boldsymbol{V}_H = \frac{\boldsymbol{I_x B_z}}{\boldsymbol{nte}} \tag{2.6}$$

and it can be transformed to Equation 2.7:

$$\boldsymbol{n} = \frac{\boldsymbol{I_x B_z}}{\boldsymbol{V_H te}} \tag{2.7}$$

The current in x direction is $\boldsymbol{I}_x$, the magnetic field in z direction is $\boldsymbol{B}_z$, the Hall voltage and thickness t are all measurable while e is a constant. Thus, by using the above equations, the carrier density $\boldsymbol{n}$ can be calculated.

2.1.2 Metal–Oxide–Semiconductor Field-Effect Transistor

In order to perform experimental research on the electrical properties of MoS_2 and WS_2, the corresponding devices need to be fabricated first. In most of the experimental research on TMDCs, Metal–Oxide–Semiconductor Field-Effect Transistor is the most commonly chosen device for fabrication. Thus, a brief introduction to the MOSFET is necessary.

MOSFET is a special type of transistor which is widely used in circuits. The main advantage of MOSFET over other transistors is that it only requires a diminutive current to turn on and deliver a large current. MoS_2-based FETs have exhibited high ON/OFF ratio - higher than 10^8 which means that the process of turning the switch can be performed in a very short time; thus, this indicates the potential application of MoS_2 in future electronic devices[11, 12]. Meanwhile, WS_2-based FETs show the highest electron mobility among all the TMDCs[13].

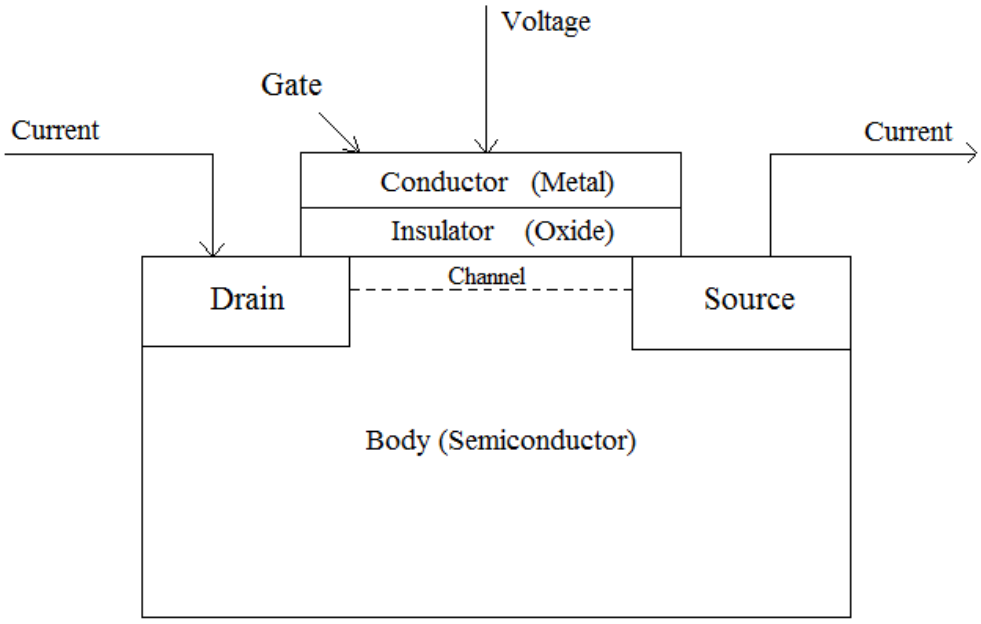

Figure 2.2 Schematic of a simple MOSFET

As shown in Figure 2.2, a MOSFET has four terminals, which are source(S), gate (G), drain (D) and body (B), while normal field effect transistors only have three terminals, which are gate, source and drain. The conductor and insulator layer form the gate together,

while source, drain and body are all formed by the semiconductor. It is notable that drain and source should be the same type of semiconductor while the type of semiconductor in the body should be different from the former. Metal in the MOSFET is always a misnomer since polycrystalline silicon has been adapted as the gate material. This also applies to the oxide in the MOSFET, which can be replaced by other dielectric materials. In normal situation, the different semiconductor types between drain and body cause a depletion region at the boundary between them where no charge carriers can pass. For instance, assuming that the drain and source are p-type semiconductors while body is an n-type semiconductor, the electrons in n-type semiconductor body will fill the holes in p-type semiconductor drain and source to a certain depth; thus, regions with no charge carriers are created between drain and body. The switch between drain and source is off.

2.2 Experimental Research

2.2.1 MoS_2

Charge carrier mobility in bulk MoS_2, at room temperature, has been studied by Fivaz and Mooser in 1967. Their results show that the charge carriers can reach mobility in the range of 200-500 cm^2/Vs [14]. Recently, experiments have been carried out on monolayer MoS_2 at room temperature. It should be noted that the mobility decreased to 0.1-10 cm^2/Vs [11, 15]. The main reason for the decrease is the charge traps at the interface between MoS_2 and the substrate[16].

In order to increase the mobility of MoS_2 in FET at room temperature, the understanding of the transition mechanism is very important. In 2013, Radisavljevic et al.

reported their study on the mobility measurements in monolayer MoS_2, based on Hall effect[17]. In their study, the mobility of MoS_2 in FET are measured at different temperatures, and the results are fitted to the theoretical equations to study the current conduction mechanism.

Figure 2.3 presents the structure of MoS_2 FET which is commonly fabricated and studied. In this MOSFET structure, M is MoS_2, O is SiO_2, S represents Si corresponding to Figure 2.2. The degenerately-doped Si wafer back-gate is covered by 270 nm SiO_2.

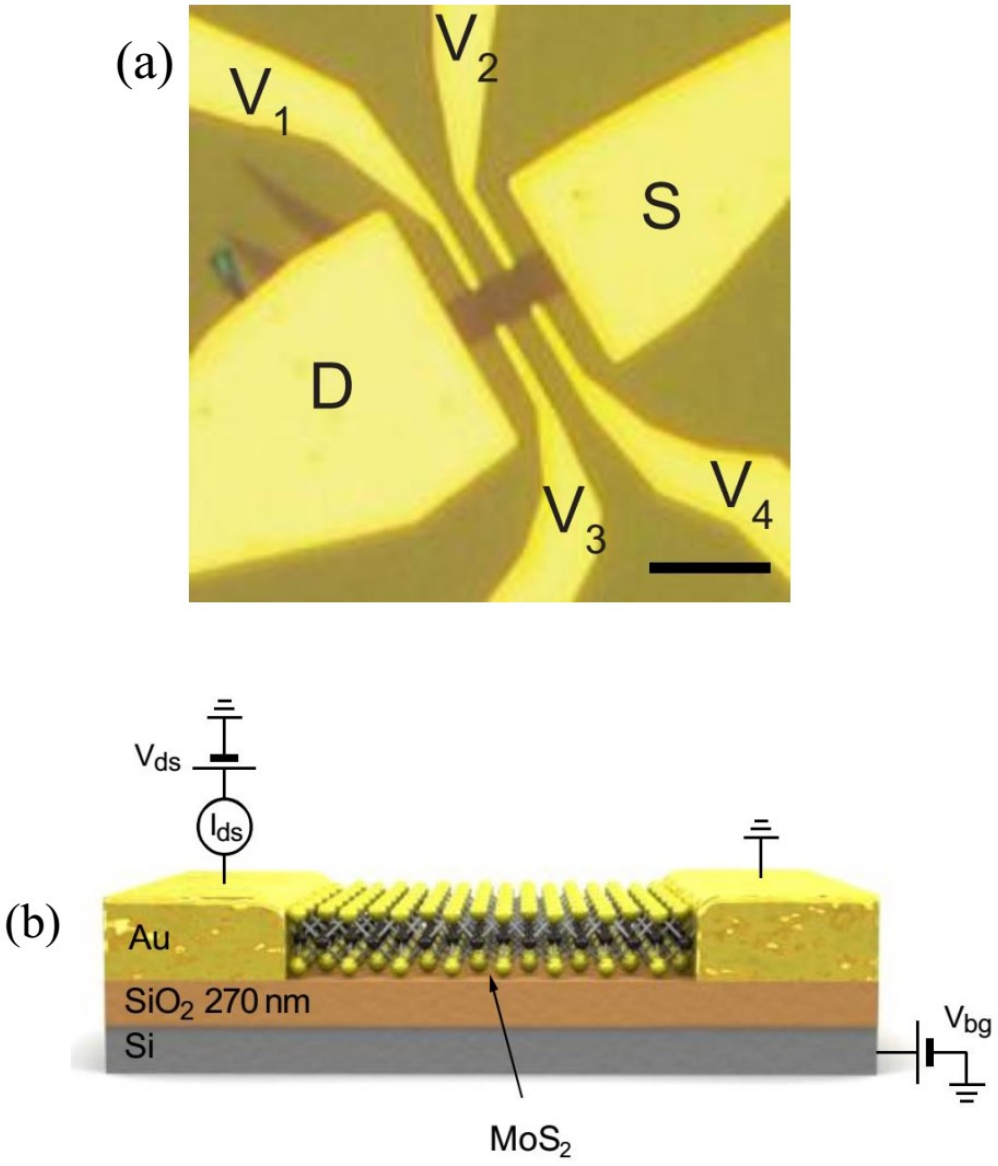

Figure 2.3 Structure of MoS_2 FET. (a) Optical image. (b) Cross section view. V_{ds} is drain-source voltage. I_{ds} is drain-source current. V_{bg} is back-gate voltage [17].

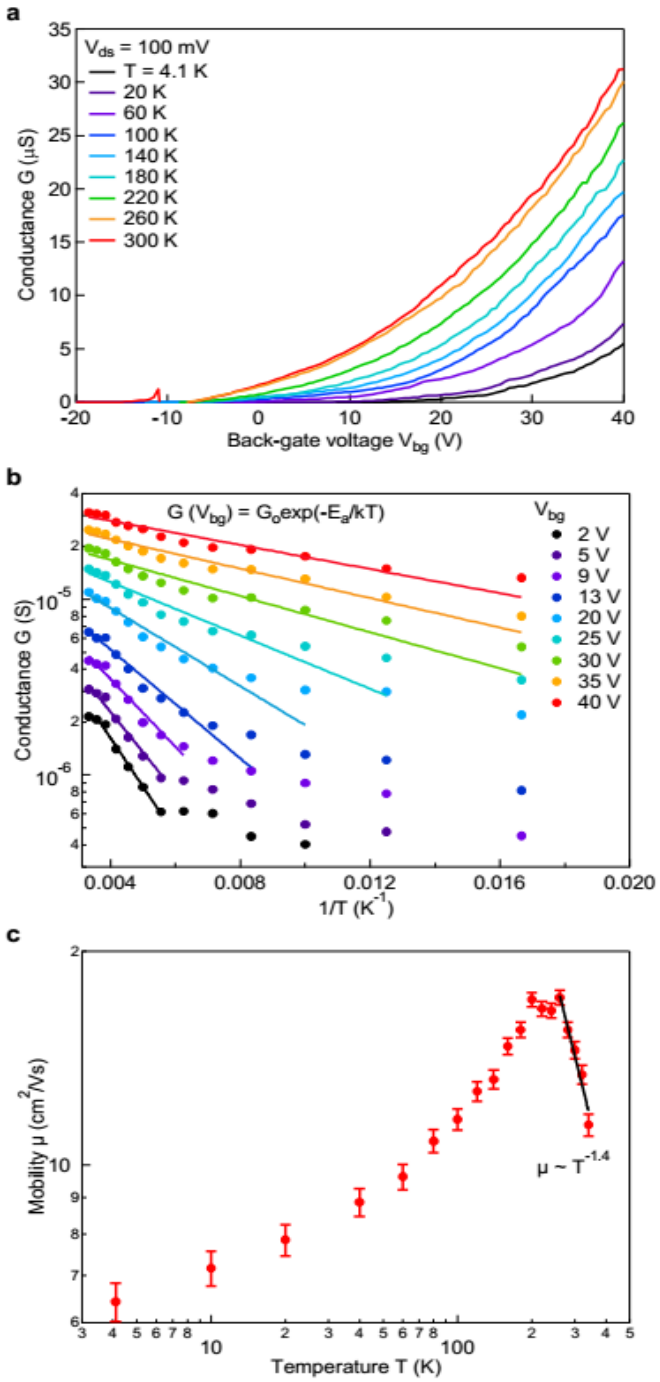

Figure 2.4 Temperature dependence of electrical properties of monolayer MoS_2

(a). Conductance G versus back-gate voltage at different temperature. (b) Conductance G versus temperature at different back-gate voltage. (c) Mobility as function of temperature [17].

The measurements in Figure 2.4 have been carried out by Hall effect. It is described in Section 2.1.1.

In Figure 2.4 a, the variation of conductance with back-gate voltage, for various device temperature is shown. For each back-gate voltage, the corresponding charge concentration can be calculated using the following equations:

$$n_{2d} = C_{ox1} * \Delta V_{bg} / e \tag{2.8}$$

$$C_{ox1} = \varepsilon_0 \varepsilon r_1 / d_{ox1} \tag{2.9}$$

$$\Delta V_{bg} = V_{bg} - V_{bg,th} \tag{2.10}$$

The $V_{bg,th}$ is the threshold voltage for each device and is close to its pinch-off voltage estimated from the conductance curves. For instance, the highest back-gate voltage of 40V corresponds to a charge concentration of $n_{2d} \sim 3.6*10^{12}$ cm^{-2}.

As shown in Figure 2.4 b, for each V_{bg}, in a certain temperature range, the conductance follows the Equation 2.11:

$$G = G_0 * \exp(\frac{-Eg}{kT}) \tag{2.11}$$

Equation 2.11 is valid for the condition when electron transport is thermally-activated; good agreement of the experimental data with Equation 2.11 shows that the electron transport in these temperature ranges are thermally activated. At lower temperatures, we can notice that the variation in conductance is weakened for all V_{bg}. This is due to hopping through localized states which becomes a dominant mechanism of electron transport, and the system approaches the localized regime.

In Figure 2.4 c, the mobility dependence on temperature is presented. The results are extracted from Figure 2.4 a and Figure 2.4 b in the range of 30-40V of back-gate voltage, V_{bg}. The flowing equation is applied in the calculation:

$$\mu=[dG/dV_{bg}]*[L_{12}/(WC_{ox1})] \quad (2.12)$$

A sharp peak corresponding to 18 cm^2/Vs is observed at 200K; after the peak, the mobility decreases with temperature. This shows that electron-phonon scattering becomes the dominant mechanism. The decreasing component of the curve can be fitted in accordance with $\mu \sim T^{\gamma}$, $\gamma \approx -1.4$, which is in agreement with the theoretical predictions of $\gamma \approx -1.69$[18].

2.2.2 WS_2

WS_2 is also an important member of the TMDC class of materials. In 2011, Liu et al. performed a theoretical study of all the TMDCs. Among all these materials, WS_2 shows the highest mobility which results from its reduced effective mass[19]. A recent report estimates that monolayer WS_2 exhibits 44 $cm^2/(Vs)$ mobility at room temperature[20]. Similar to MoS_2, the temperature dependence study of the electrical properties of WS_2 is critical for understanding the current conduction mechanism which is key to improving its performance. In 2014, temperature dependent mobility study of WS_2 based devices was performed by Ovchinnikov et al. [21]. In this study, the mobility of WS_2 in FET, at different temperatures, are measured, and the results are fitted to the theoretical equations to study the conduction mechanism.

Due to similarity between the studies on MoS_2 and WS_2, a detailed mathematical method of WS_2 will not be discussed here.

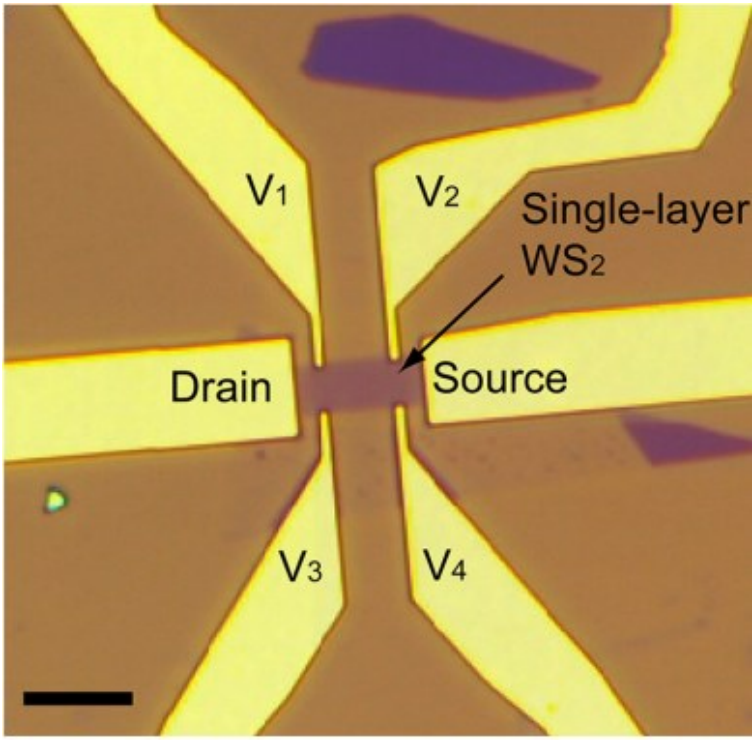

Figure 2.5 Optical image of WS_2 FET [21].

Figure 2.5 shows the optical image of WS_2. As can be seen in this figure, it is almost the same as the in the case of MoS_2 FET. Si.is chosen as the back-gate material and a 270 nm thick SiO_2 is chosen as the oxide on Si.

In Figures 2.6 a and b, the variation of sheet conductivity with gate voltage, as function of temperature is shown. Sheet conductivity and conductance can be transformed to each other utilizing the equation:

$$G = \sigma * t \qquad (2.13)$$

It is observed that in Figure 2.6 a, when V_g is below 70V, the sheet conductivity increases with increase in temperature. However, when V_g is greater than 70V, the sheet conductivity decreases with increase in temperature. This indicates a transition from insulator regime to conductor regime.

Thus, Figures 2.4 and 2.6 show the same properties of MoS_2 and WS_2. In Figure 2.6 c, the mobility decreases with increasing temperature for WS_2, which is different from MoS_2. In MoS_2, there emerges a sharp peak, while in WS_2, no peak is formed.

This shows significant difference in the conduction mechanism of the two materials for low temperatures. At higher temperatures, WS_2 shows a power-law dependence; the experiment shows that $\mu \sim T^{\gamma}$, $\gamma \approx -0.73$.

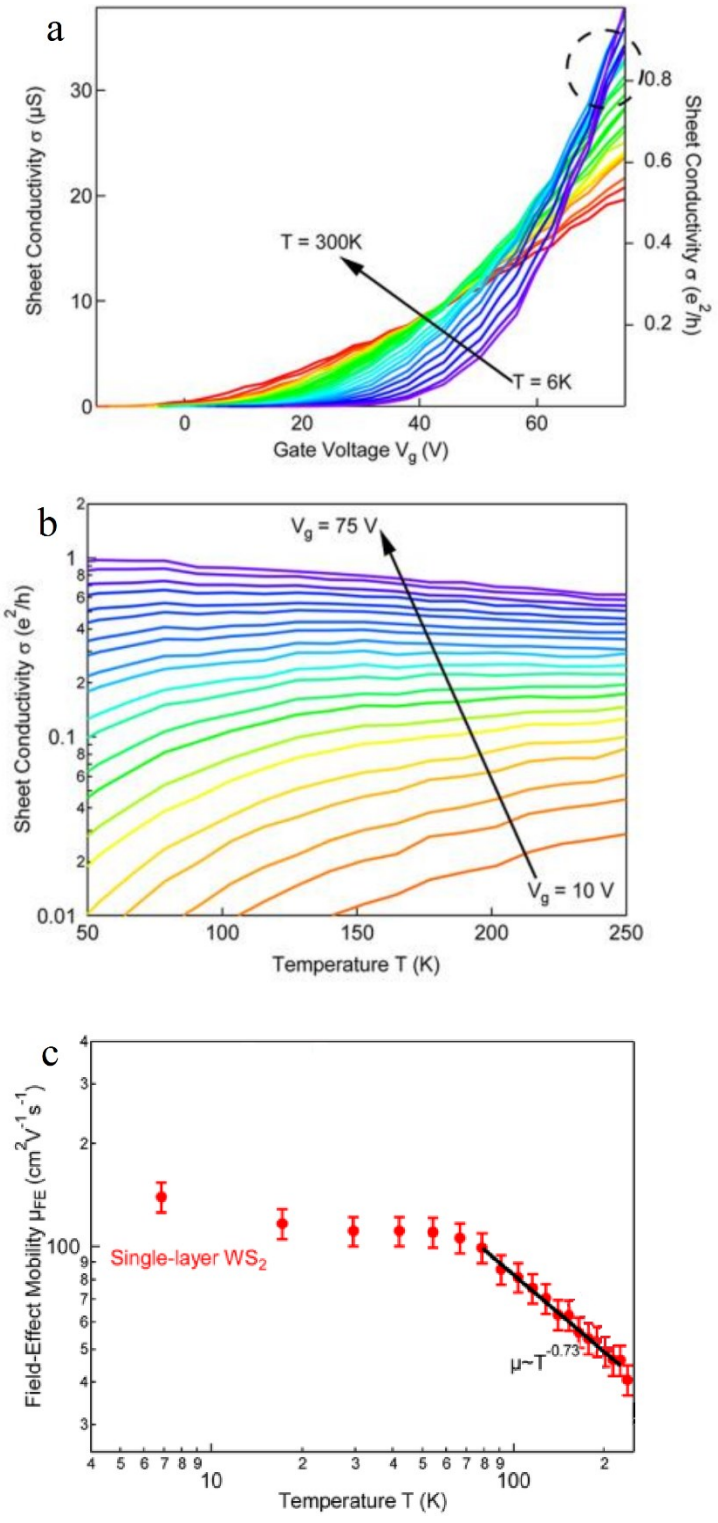

Figure 2.6 Temperature dependence of electrical properties of monolayer WS_2
(a). sheet resistivity versus back-gate voltage at different temperature.
(b) Sheet resistivity versus temperature at different back-gate voltage.
(c) Mobility dependence on temperature [21].

2.3 Conclusion and Future Study

In this chapter the electrical properties of monolayer MoS_2 and monolayer WS_2 measured by experiment have been presented. Unlike theoretical simulation results by first principle study, the experimental results show a much lower mobility for both MoS_2 and WS_2. This difference is due to many factors, and it is necessary to perform more study to solve the problem. As mentioned before in Section 2.2, the study of conducting mechanism is an important part in understanding and solving the difference. Since monolayer MoS_2 and WS_2 have ultra-thin thickness, the influence of substrate is also an essential part.

In future studies, experiments with different substrates should be carried out to study the influence of substrate on the monolayer MoS_2 and monolayer WS_2. Also, the interface geometry of these 2-D materials and substrate should be future investigated[22]. The above two study direction should help in understanding and solving the problem to enhance the future application.

CHAPTER 3

ELECTRONIC PROPERTIES OF MoS_2 and WS_2

In this chapter, a literature review of the electronic properties of MoS_2 and WS_2 with a focus on the band structure of these two materials, as function of number of layers, is presented. The temperature dependence of the band gap of MoS_2 and WS_2 monolayers are investigated by MATLAB simulations.

3.1 Band Structure of MoS_2 and WS_2

The band structure is very important in understanding the properties of materials and finding possible applications. The reduction in the number of layers causes significant changes to the band structure of both the materials and the special band structure of monolayer MoS_2 and WS_2 has drawn the attention of scientists.

3.1.1 Electronic Band Structure

The electronic band structure (or band structure) of a solid describes the range of energies that the electrons within the solid can possess, and the range of energy states that they may not possess. Due to quantum mechanical wave functions, the electrons in the solid can only possess certain range of energy in certain locations in the band structure.

The repetitiveness of the periodic lattice, which is described by the Brillouin zone, allows utilizing the band structure of a lattice to represent the band structure of the entire solid. The band theory has been utilized to explain many important physical properties and is essential in designing all the electrical devices.

3.1.2 Brillouin Zone

Brillouin zone is often used in mathematics and solid state physics to describe the primitive cell in reciprocal space. The reciprocal lattice is broken into Brillouin zones as the Bravais lattice is broken into cells. The solution to the Bloch wave in a periodic medium can be represented by their behavior in a single Brillouin zone.

MoS_2 and WS_2 are both comprised of hexagonal lattice, which is presented in Figure 3.1 to give a better understanding of the electronic band structure of MoS_2 and WS_2.

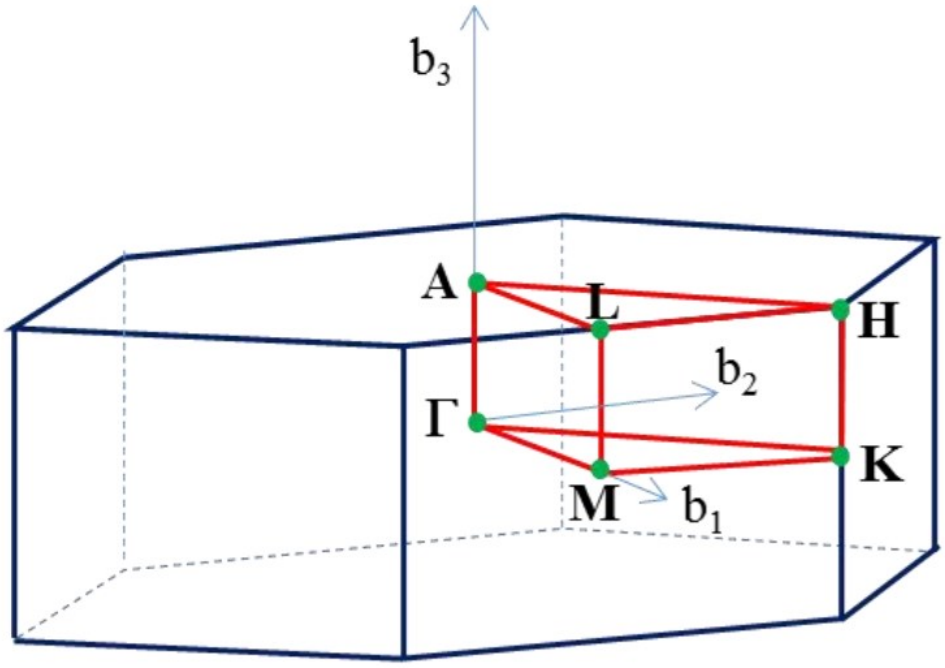

Figure 3.1 The Brillouin zone and special point of the hexagonal lattice system for MoS_2 and WS_2. A is the center of a hexagonal face, H is the corner point, K is the middle of an edge joining two rectangular faces, L is the middle of an edge joining a hexagonal and a rectangular face, M is the center of a rectangular face, Γ is the center of the Brillouin zone [23].

3.1.3 Band Structure of MoS_2 and WS_2

In 2012, A. Kumar and P.K. Ahluwalia have performed a thorough investigation of the electronic structure of all TMDCs utilizing first principle calculations, and their results are in good agreement with the experimental measurements[24].

Figure 3.2 shows the band structure of MoS_2, as function of the number of layers. As can be seen in the figure, bulk MoS_2 has an indirect band gap of 0.75eV. However, with the decreasing number of layers, the value of the indirect band gap increases. As the number of layers reaches one, the location of the band gap shifts and the monolayer MoS_2 becomes a direct band gap semiconductor with a band gap of 1.89eV. The corresponding blue shift is 1.14eV.

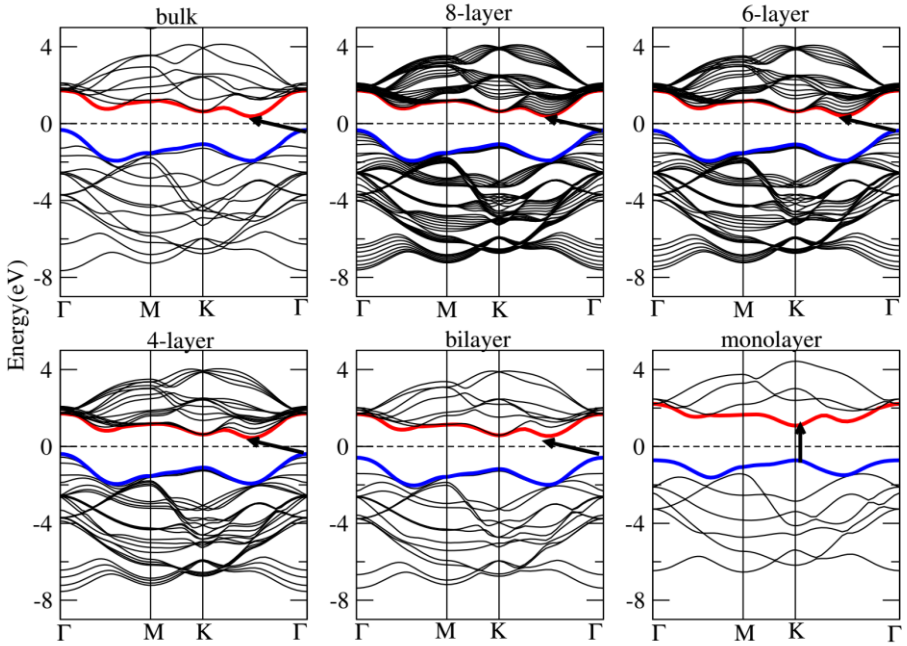

Figure 3.2 Band structure of MoS_2 as function of number of layers. The arrow represents the approximate location of the band gap. The symbols in the Figure are illustrated in Figure 3.1 [24].

The value of blue shift is even larger than the value of the indirect band gap of the bulk MoS_2. This indicates that there will be a huge change in the properties of the monolayer MoS_2.The location of the band gap also changes; both the maximum valence band and the minimum conduction band are located at the K point in the Brillouin zone (the middle of an edge joining two rectangular faces) in monolayer MoS_2. The reduced number of layers cause the band gap of MoS_2 to shift from infrared region towards visible region and switch the type of the band gap from indirect to direct. These changes lead to potential applications of monolayer MoS_2 for optoelectronic devices.

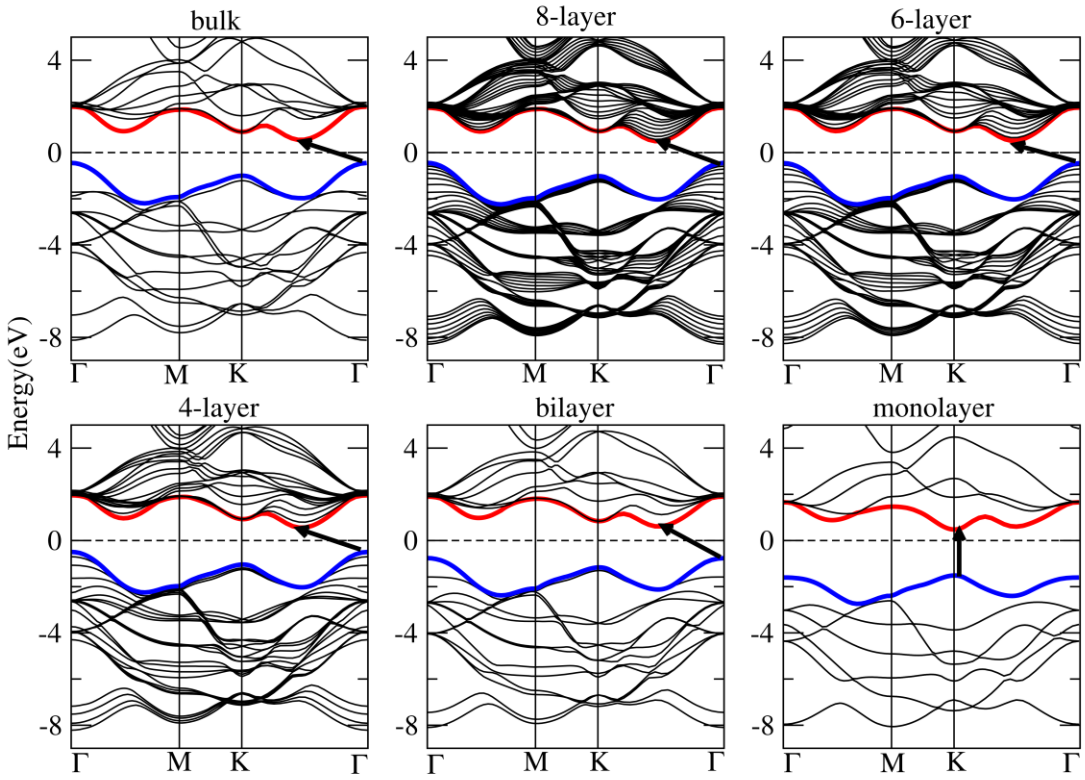

Figure 3.3 Band structure of WS_2 as function of the number of layers. The arrow represents the transition from the highest valence band to the lowest conduction band. The symbols in this figure are illustrated in Figure 3.1 [24].

Figure 3.3 shows the band structure of WS_2 as function of the number of layers. Generally, the change in band structure of WS_2 is similar to that of MoS_2. Different from MoS_2, the value of the indirect band gap in bulk WS_2 is 0.89eV, while the value of the direct band gap in monolayer WS_2 is 2.05. The value of the blue shift is 1.16eV.

The variation in the value of band gaps is concluded in Figure 3.4. It should be noted that the value of the direct band gap at K point hardly varies with the number of layers, while the indirect band gap varies drastically with the number of layers from one layer to four layer.

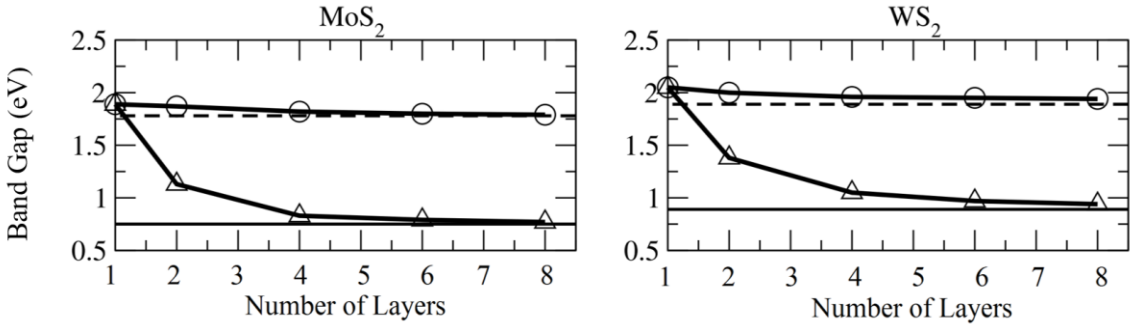

Figure 3.4 The value of direct and indirect band gap in MoS_2 and WS_2. The solid lines with triangles are for indirect band gap, while the solid lines with circles are for direct band gap at K point [24].

3.2 Temperature Dependence of Band Gap in Monolayer MoS_2 and WS_2

The properties of semiconductor devices are very sensitive to temperature, and thus, the knowledge of the influence of temperature change on the band gap is essential. Generally, the energy gap of a semiconductor tends to decrease with increase in temperature. As the thermal energy increases, the amplitude of the atomic vibrations increases leading to increase in the atomic spacing[25]. Therefore, an increased interatomic spacing decreases

the potential seen by the electrons in the material, which in turn reduces the size of the energy gap[25]. The relationship between temperature and band gap can be expressed by Equation 3.1 which is formulated by O'Donnell; the equation serves to be a direct replacement of Varshini's equation[26].

$$E_g(T) = E_g(0) - S\langle\hbar\omega\rangle[\coth\langle\hbar\omega\rangle/2kT) - 1] \quad (3.1)$$

$E_g(0)$ is the band gap of the semiconductor at 0 K, S is a dimensionless coupling constant and $\langle\hbar\omega\rangle$ is an average phonon energy. This equation was explicitly used due to poor fitting results obtained from using full theoretical treatments[25].

Table 3.1 Fitting Parameters of E_g for Monolayer MoS_2 and WS_2

Material	$E_g(0)$ (eV)	S	$\langle\hbar\omega\rangle$ (meV)	References
MoS_2	1.86	1.82	2.25	[27]
WS_2	2.08	2.47	1.30	[28]

Table 3.1 shows the fitting parameters of monolayer MoS_2 and monolayer WS_2 based on Equation 3.1. By introducing these parameters into Equation 3.1, the variation of the band gap with temperature are plotted in Figure 3.5.

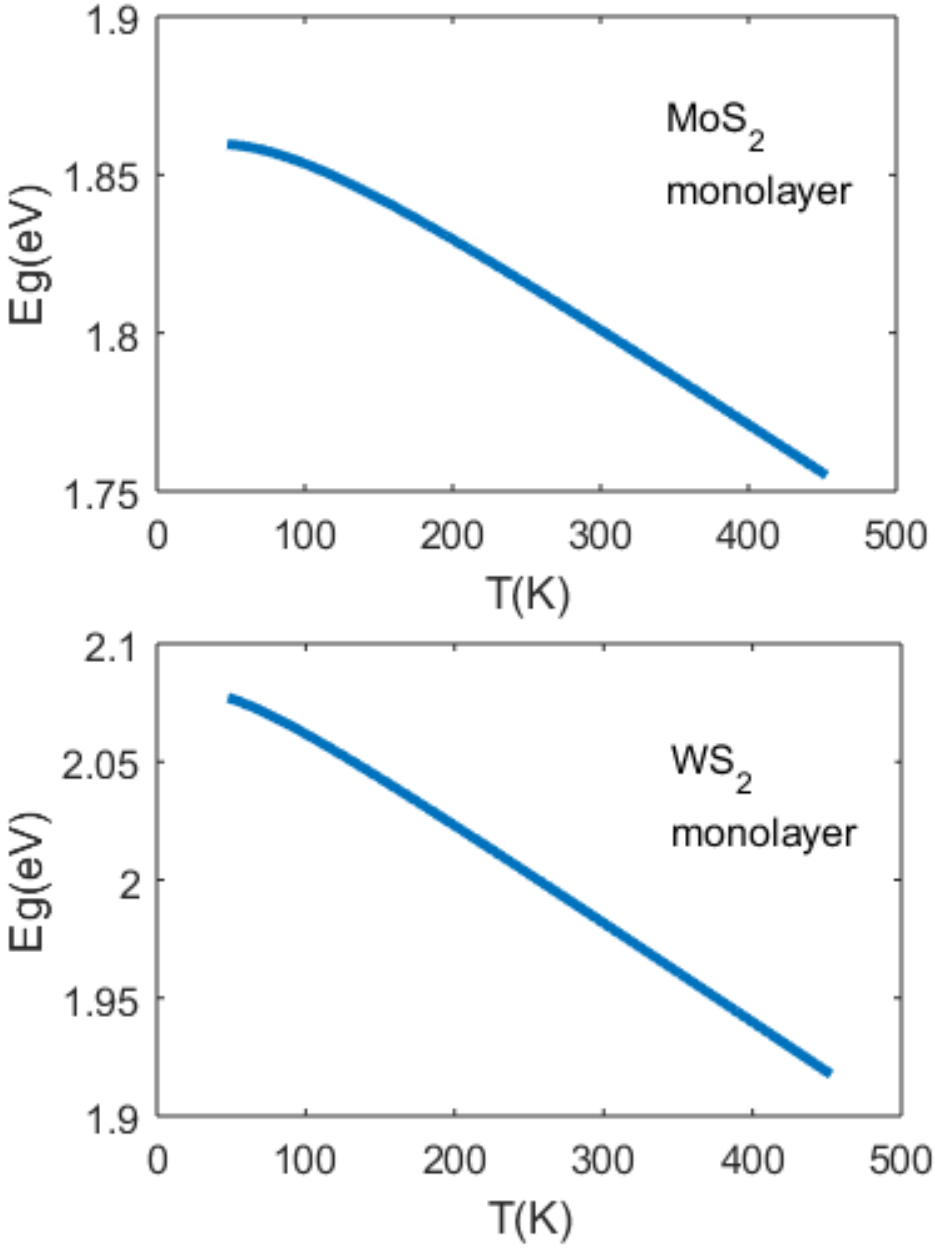

Figure 3.5 Temperature dependence of band gap for monolayer MoS_2 and monolayer WS_2.

As shown in Figure 3.5, the variation in band gap versus temperature is generally a straight line except for the initial low temperature part. The band gap decreases significantly with the change in temperature. In order to have a better understanding of the

relationship between band gap and temperature, dE_g/dT versus T is also plotted as Figure 3.6.

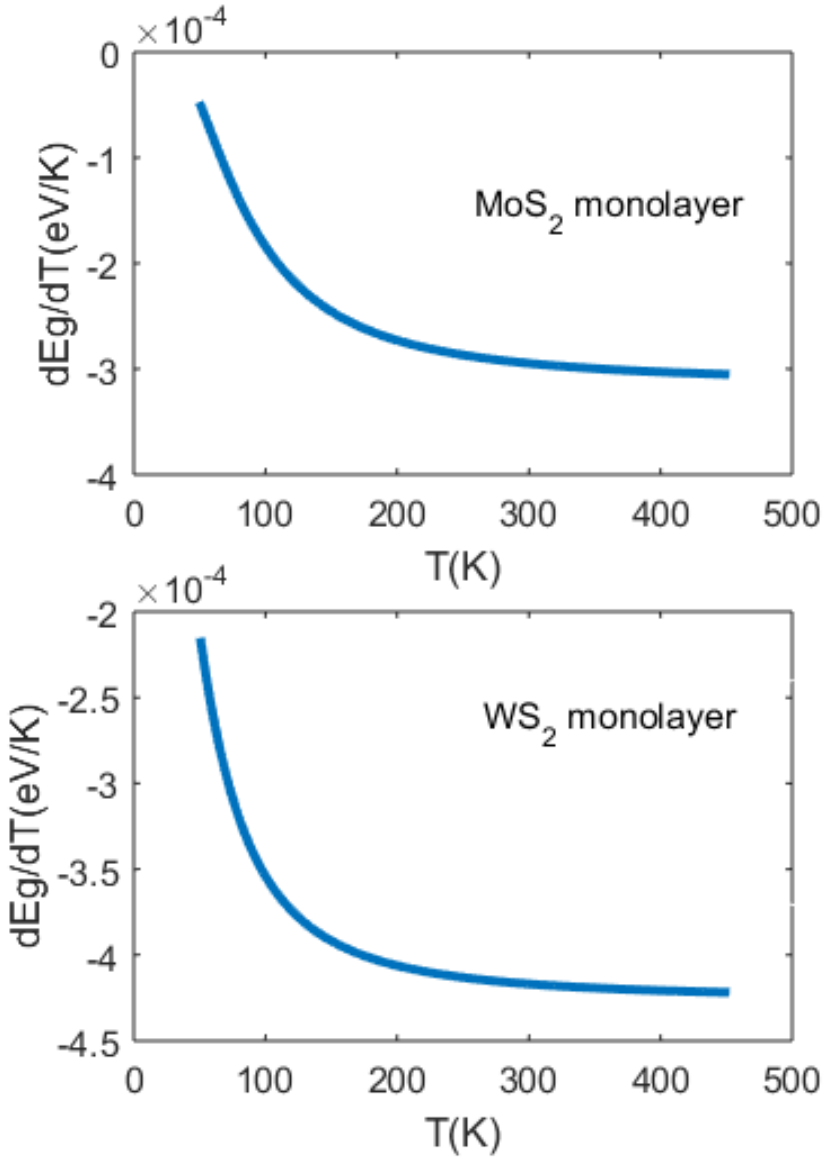

Figure 3.6 $\frac{dE_g}{dT}$ of monolayer MoS_2 and WS_2

CHAPTER 4

OPTICAL PROPERTIES OF MoS_2 and WS_2

In recent years, there has been a large volume of research conducted on the optical properties of TMDCs; however, much of the research revolves around the spectral reflectance, differential reflectance, differential transmittance, spectral absorptance and absorbance.

These studies are usually based on experimental research and very less or, in some cases, no simulations are carried out. Despite the intense research carried out on the optical properties of TMDCs, none of the studies give definite values of refractive indices and extinction coefficients. Furthermore, the results of most of the studies involving reflectance, absorptance and transmittance calculations are not in accord with each other and there is a large spread in the obtained data of the optical properties.

In this Chapter, the optical properties such as refractive index, extinction coefficient, absorptance, reflectance and transmittance of MoS_2 and WS_2, in the energy range of 1.50 eV to 3.00 eV, are studied by MATLAB modeling method. The optical band gap is also modeled utilizing MATLAB modeling method. To give a better perspective of future applications, the optical properties of these materials on selected substrates (gold, silicon and fused silica) are also studied utilizing MATLAB modeling method.

4.1 Optical Properties of Suspended MoS_2 and WS_2

In this work, we have determined the values of optical constants (n and k) and optical properties (R, T and A) of MoS_2 and WS_2 by means of MATLAB simulations under conditions of normal incidence. The optical band gaps of the monolayers are also determined to compare with the electronic band gap from Chapter 3.

4.1.1 Dielectric Constants of Suspended MoS_2 and WS_2

In electromagnetism, dielectric constants are also known as relative permittivity. Suppose an electric field is applied to the material, the charged particles in the material will move due to electrical force applied by the electrical field. However, the separation of different charged particles also generates an electric field which attenuates or resists the total electric field. Here, the permittivity is a measurement of the resistance of a material when an electric field is formed; it reflects how an electric field affects and is affected by a material. Vacuum space also has its permittivity, called vacuum permittivity. This is a constant, $\varepsilon_0 = 8.85419 \times 10^{-12}$ F/m. Relative permittivity or the dielectric constant, is the ratio of the permittivity of the material to the vacuum permittivity. It is a unitless quantity expressed by Equation 4.1.

$$\varepsilon_r = \varepsilon/\varepsilon_0 \tag{4.1}$$

In real situations, the applied field is always time-dependent with changing direction and strength in certain frequency. The permittivity becomes complex in these situations by Equation 4.2.

$$\varepsilon_r = \varepsilon_1 - i*\varepsilon_2 \quad (4.2)$$

ε_1 is the real part of the dielectric constant, while ε_2 is the imaginary part of the dielectric constant.

Yilei et al. [29] measured the dielectric constants for monolayer MoS_2 and WS_2 at room temperature from experimental reflectance spectra by a constrained Kramers-Kronig analysis; we have utilized these values to calculate the photon energy-dependent refractive index and extinction coefficient. As reported by Bablu et al. [30], the values determined by Yilei et al. were found to be better than the set of values determined by other authors and were hence chosen to determine the optical properties in this work.

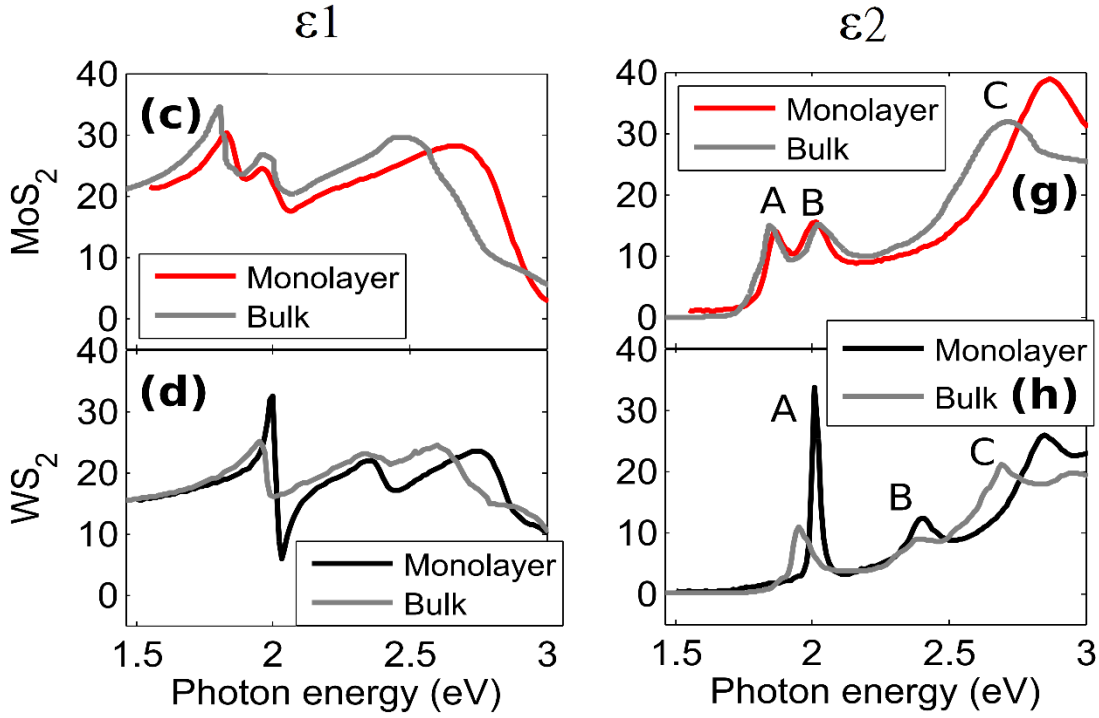

Figure 4.1 The dielectric constants of monolayer and bulk MoS_2 and WS_2, A B C are the labels of the peaks in ε_2 figures [29].

Figure 4.1 presents the results of dielectric constants of MoS_2 and WS_2 in both monolayer and bulk. It is notable that the A B points in the ε_2 – E spectra actually represent the A-B splitting of monolayer MoS_2 and monolayer WS_2. The values of the A-B splitting, determined in this method, is in agreement with the modeling results that are obtained utilizing the three-band tight-binding model[31].

4.1.2 Complex Refractive Index of Suspended MoS_2 and WS_2

When light propagates through a media, refraction and absorption will occur. The complex refractive index describes both the refraction and absorption. The complex refractive index can be expressed by the following equation:

$$n = n - ik \tag{4.2}$$

n on the left side of the equation is the complex refractive index; n on the right side of the equation is the real part of the complex refractive index and k on the right side of the equation is the imaginary part of the refractive index, also called the extinction coefficient or attenuation index.

The real and imaginary parts of the complex dielectric constant, ε_1 and ε_2, are related to the refractive index and extinction coefficient by the following two equations:

$$\varepsilon_1 = n^2 - k^2 \tag{4.3}$$

$$\varepsilon_2 = 2nk \tag{4.4}$$

Here, n and k are the refractive index and extinction coefficient of the material, respectively.

From Equations 4.3 and 4.4, we get:

$$4n^4 - 4n^2\varepsilon_1 - \varepsilon_2^2 = 0 \tag{4.5}$$

$$k = \varepsilon_2/2n \tag{4.6}$$

By solving Equation 4.5, we obtain multiple values of n; it is notable that only the real and positive value is meaningful. After n is calculated, the value of extinction coefficient k is derived from Equation 4.6.

Figure 4.2 shows the results of n and k for MoS_2 and WS_2 in both monolayer and bulk.

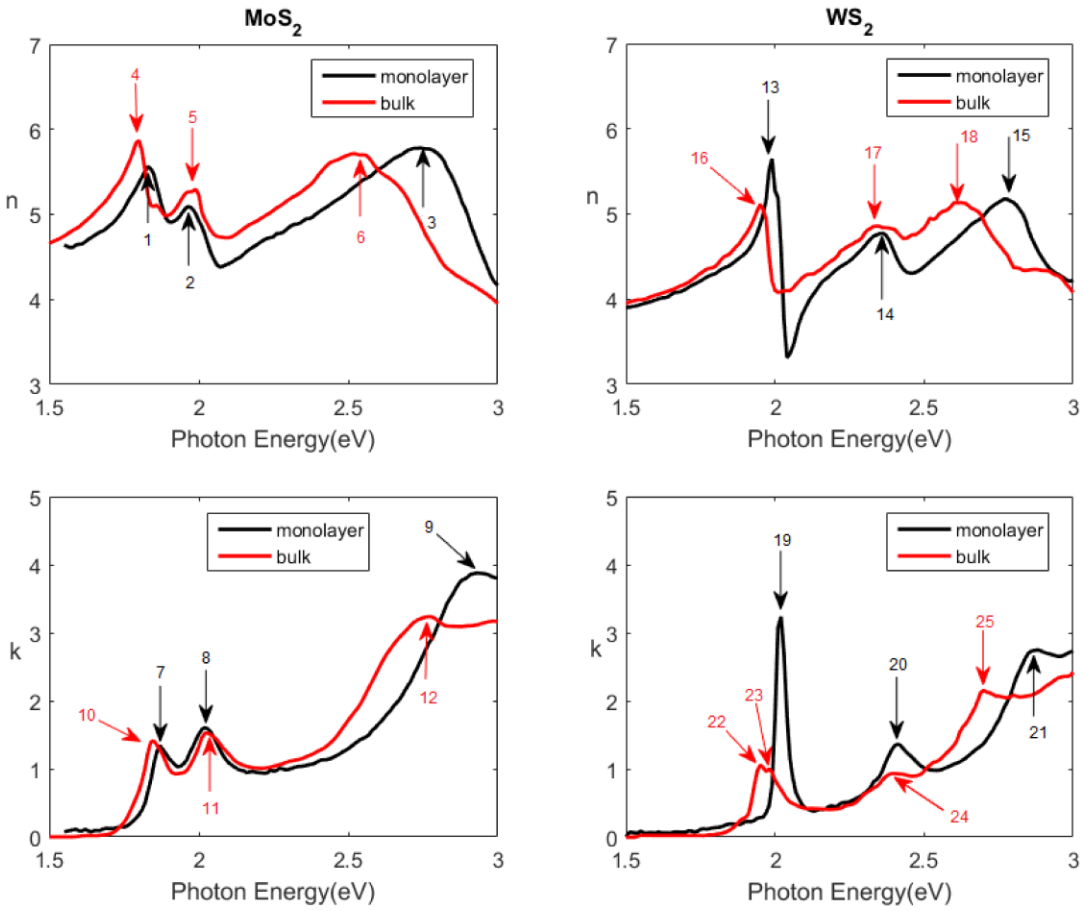

Figure 4.2 The real refractive index and extinction coefficient of suspended monolayer and bulk MoS_2 and WS_2.

Table 4.1 Energies Corresponding to Features of n(E) and k(E) for Suspended MoS_2 and WS_2

Material	No.	E(eV)	n	No.	E(eV)	k
MoS_2 monolayer	1	1.83	5.563	7	1.87	1.341
	2	1.97	5.089	8	2.02	1.607
	3	2.74	5.781	9	2.93	3.879
MoS_2 bulk	4	1.8	5.868	10	1.85	1.3411
	5	1.99	5.294	11	2.03	1.524
	6	2.52	5.714	12	2.77	3.237
WS_2 monolayer	13	1.99	5.648	19	2.02	3.237
	14	2.36	4.772	20	2.41	1.364
	15	2.77	5.176	21	2.88	2.747
WS_2 bulk	16	1.95	5.112	22	1.95	1.056
	17	2.34	4.857	23	1.98	1.002
	18	2.62	5.133	24	2.4	0.933
				25	2.7	2.154

In order to give a better understanding of Figure 4.2, the significant features are presented in Table 4.1.

4.1.3 Reflectance Transmittance and Absorptance of Suspended MoS_2 and WS_2

When a beam of light penetrates a medium, the energy of the beam will be reflected by the surface of the medium, transmitted through the medium and absorbed by the medium. The reflectance, transmittance and absorptance are respectively corresponding to the above three phenomena. They represent the fraction of the incident electromagnetic power that is reflected, transmitted and absorbed by the medium. This also means that their sum total will be 100%.

These fractions are decided by the incident energy, the incident angle and the properties (or the complex refraction index and thickness) of the medium. It should be noted that, in this study, all the simulations are carried out in vertical incidence and room temperature. The range of the incident energy is 1.50eV to 3.00eV (wavelength 826.7nm to 413.3nm).

The reflectance, transmittance and absorptance are related to the complex refractive index and thickness of the medium by the following equations.

$$R = \frac{(n-1)^2 + k^2}{(n+1)^2 + k^2} \tag{4.7}$$

$$\lambda = \frac{hc}{E} \tag{4.8}$$

$$\alpha = \frac{4\pi k}{\lambda} \tag{4.9}$$

$$T = (1 - R)(e^{-\alpha t}) \tag{4.10}$$

$$A = 1 - R - T \tag{4.11}$$

α in Equations 4.7 and 4.9 is called the absorption coefficient, which describes the absorbing ability of a material in certain energy. λ, in Equations 4.8 and 4.9 is the wavelength of the incident light. t in Equation 4.10 is the thickness of the material. R is reflectance, T is transmittance and A is absorptance. The reflectance is independent of the thickness of the medium; it is only a surface property. However, transmittance and absorptance are closely related to the thickness of the medium. When light penetrates longer distance through the medium, more energy is absorbed by the medium.

The thickness of monolayer MoS_2 and WS_2 were considered as 0.65nm[4]. The thickness of bulk MoS_2 and WS_2 were taken as 20nm, which seemed to be the optimal value[32]. Based on the above equations, the reflectance, transmittance and absorptance of monolayer and bulk MoS_2 and WS_2 are simulated and presented in Figure 4.3.

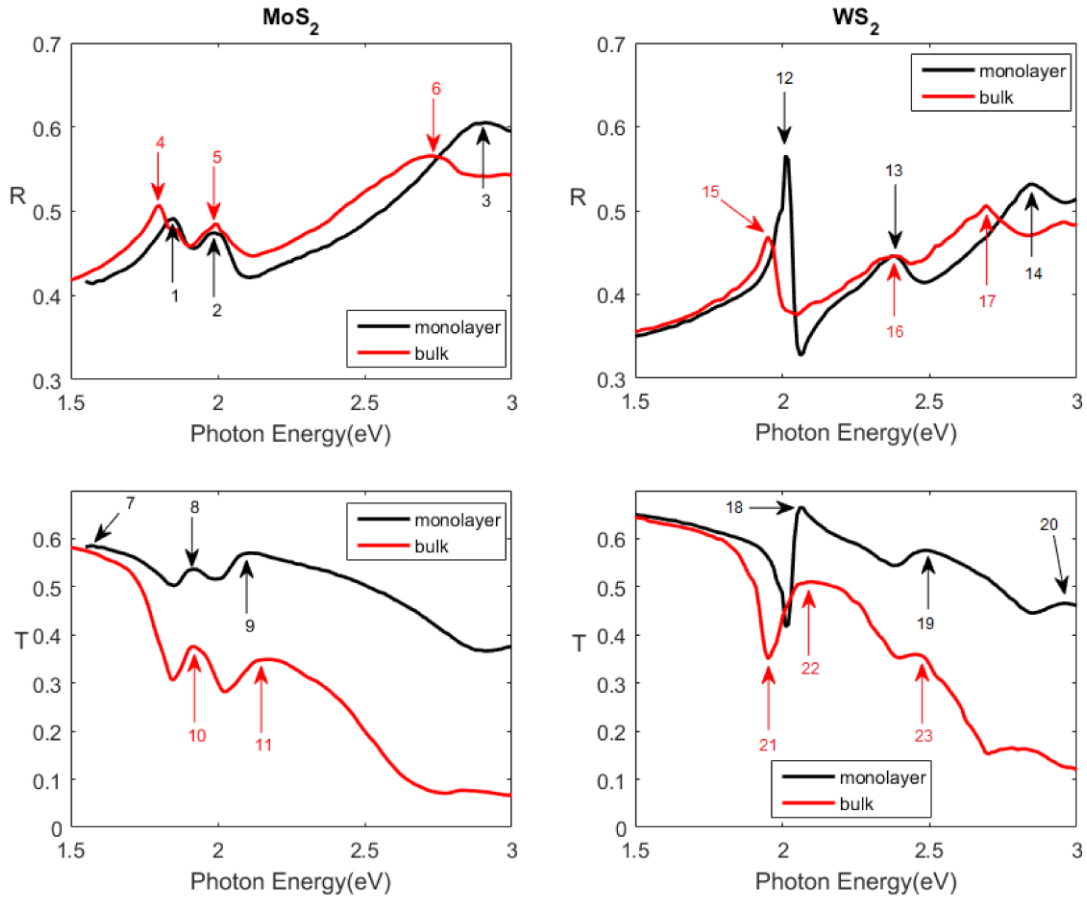

Figure 4.3 Simulated reflectance and transmittance of monolayer and bulk MoS_2 and WS_2.

The simulated reflectance and transmittance spectra, under conditions of normal incidence and room temperature, are presented in Figure 4.3. For all four monolayer and bulk TMDCs, the two lowest energy peaks in the reflectance spectra correspond to the excitonic features associated with inter-band transitions in the K (K') point in the Brillouin zone[10]. The two significant peaks in Figure 4.3 can be attributed to the splitting of the valence band by spin-orbit coupling, including the transitions near the Γ point[33, 34].

The maximum value of Reflectance (R) and the corresponding energy (E) for monolayer MoS_2 and WS_2 are as follows: 60.5% (2.91 eV) and 56.5% (2.01eV),

respectively. Similarly, the maximum value of R for bulk MoS_2 and WS_2 are as follows: 50.7% (1.8 eV) and 50.6% (2.69 eV), respectively.

For the simulated transmittance spectra, the maximum values of Transmittance (T) and the corresponding energy (E) for monolayer MoS_2 and WS_2 are as follows: 57% (2.11 eV) and 66.5% (2.06eV) respectively. Similarly, the maximum value of T for bulk MoS_2 and WS_2 are 37.6% (1.92 eV) and 51.9% (1.79 eV), respectively.

Simulated absorptance spectra are shown in Figure 4.4. The spectra of monolayer and bulk are separated due to the large change in the magnitude of absorptance value of monolayer and bulk. This change is reasonable due to the increase in the number of layers which leads to increase in absorptance of light by the material.

Within the range of photon energy considered in this study, as observed from Figure 4.4, the maximum values of Absorptance (A) in the energy range for monolayer MoS_2 and WS_2 are as follows: 2.93% and 2.55%, respectively. Similarly, the maximum value of A for bulk MoS_2 and WS_2 are as follows: 39.1% and 39.7%, respectively. The location of the peaks in either case remains relatively similar; these peaks are the A and B exciton absorption peaks which originate from the spin-split direct gap transitions at the K point of the Brillouin zone.

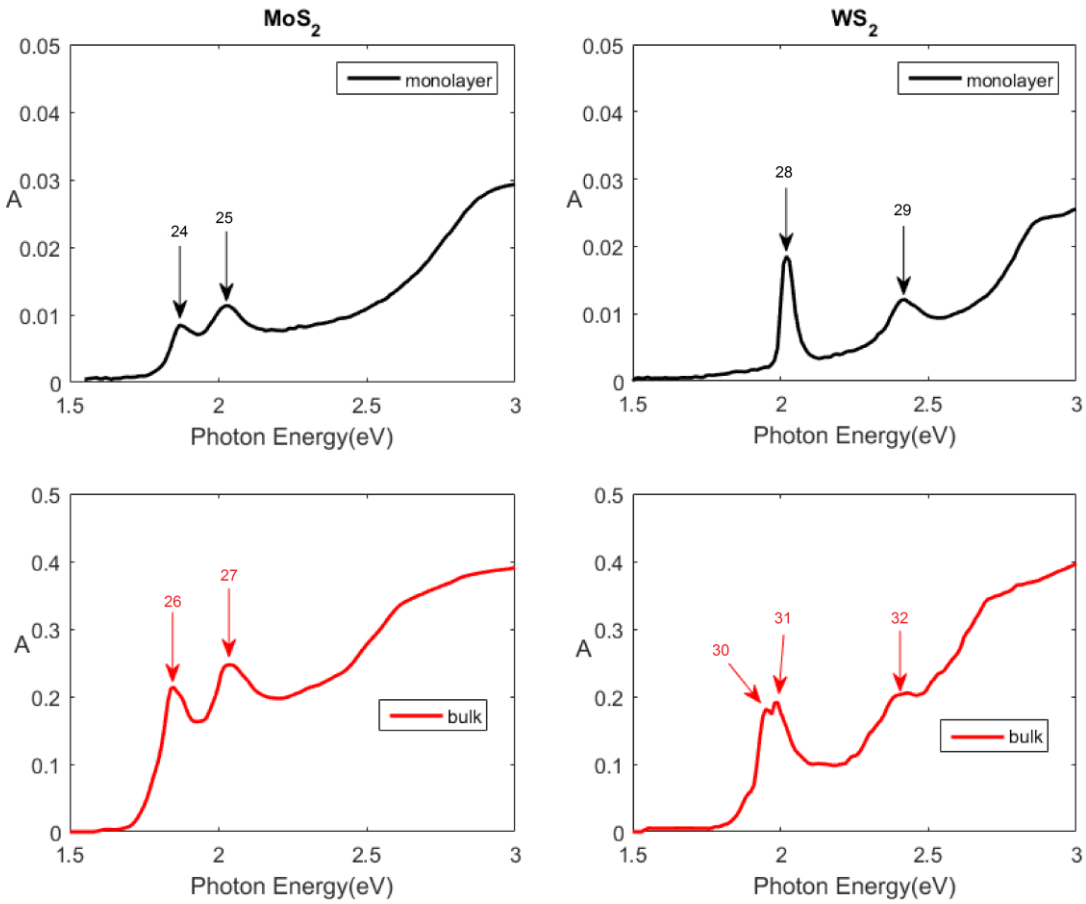

Figure 4.4 The simulated absorptance of monolayer and bulk MoS_2 and WS_2.

All the values corresponding to features, present in Figures 4.3 and 4.4, are listed in Table 4.2.

Table 4.2. Energies Corresponding to Features of R, T and A for Monolayer and Bulk MoS_2 and WS_2

Material	No.	E(eV)	R	No.	E(eV)	T	No.	E(eV)	A
MoS_2	1	1.85	0.491	7	1.57	0.585	24	1.87	0.00848
monolayer	2	1.99	0.474	8	1.92	0.537	25	2.03	0.01135
	3	2.91	0.605	9	2.11	0.57			
MoS_2 bulk	4	1.8	0.507	10	1.92	0.376	26	1.85	0.214
	5	1.99	0.485	11	2.17	0.349	27	2.04	0.247
	6	2.73	0.566						
WS_2	12	2.01	0.565	18	2.06	0.665	28	2.02	0.0185
monolayer	13	2.38	0.446	19	2.49	0.576	29	2.41	0.0121
	14	2.85	0.531	20	2.96	0.466			
WS_2 bulk	15	1.95	0.469	21	1.95	0.35	30	1.95	0.181
	16	2.38	0.446	22	2.1	0.51	31	1.99	0.191
	17	2.69	0.506	23	2.45	0.359	32	2.43	0.205

4.1.4 Optical Band Gap of Monolayer and Bulk MoS_2 and WS_2

As mentioned in Chapter 3, the band gap is an essential property of a material. For monolayer MoS_2 and WS_2, their direct band gaps in the visible range make them promising in a variety of applications in optoelectronics. The band gap generally refers to the energy difference between the bottom of the conduction band and the top of the valence band.

There are generally two methods of measuring the band gap of a material. One can measure the band gap optically by excitation spectroscopy in which the charge state of the material is not changed. The band gap, measured in this method, is called optical band gap. One can also measure the band gap through electron spectroscopy like photoemission for the valence band and inverse photoemission for the conduction band. In this method, an electron is either injected into the solid or removed from the solid. This is called electrical band gap.

Utilizing the absorptance versus energy measured in Section 4.1.3, the optical band gap of a material can be determined. By plotting certain powers of the absorption coefficient against photon energy, one can normally confirm the value of the band gap, and whether or not it is direct. If a plot of α^2 versus photon energy forms a straight line, it can normally be inferred that the band gap is direct, measurable by extrapolating the straight line to $\alpha=0$ axis. On the other hand, if a plot of $\alpha^{1/2}$ versus photon energy forms a straight line, it can normally be inferred that the band gap is indirect, measurable by extrapolating the straight line to $\alpha=0$ axis.

The monolayer MoS_2 and WS_2 are examined for the direct semiconductor case. Figure 4.5 presents the square of the absorption versus energy.

As seen from Figure 4.5, we observe a straight line behavior near the first peaks of the two monolayers; this shows that the monolayer MoS_2 and WS_2 have a direct band gap. The values of the optical band gap of monolayer MoS_2 and WS_2 were obtained by solving the equations to straight lines. The optical band gaps of monolayer MoS_2, WS_2 are 1.82 eV and1.98 eV, respectively. The calculated optical band gaps are smaller than the electronic band gaps in Chapter 3 within a reasonable range; this is due to the additional energy absorbed by an electron while making a transition from the valence band to the conduction band; there is a difference in the coulomb energies of the two systems (excitation spectroscopy and tunneling spectroscopy) which, therefore, causes a change in the optical band gaps and electrical band gaps.

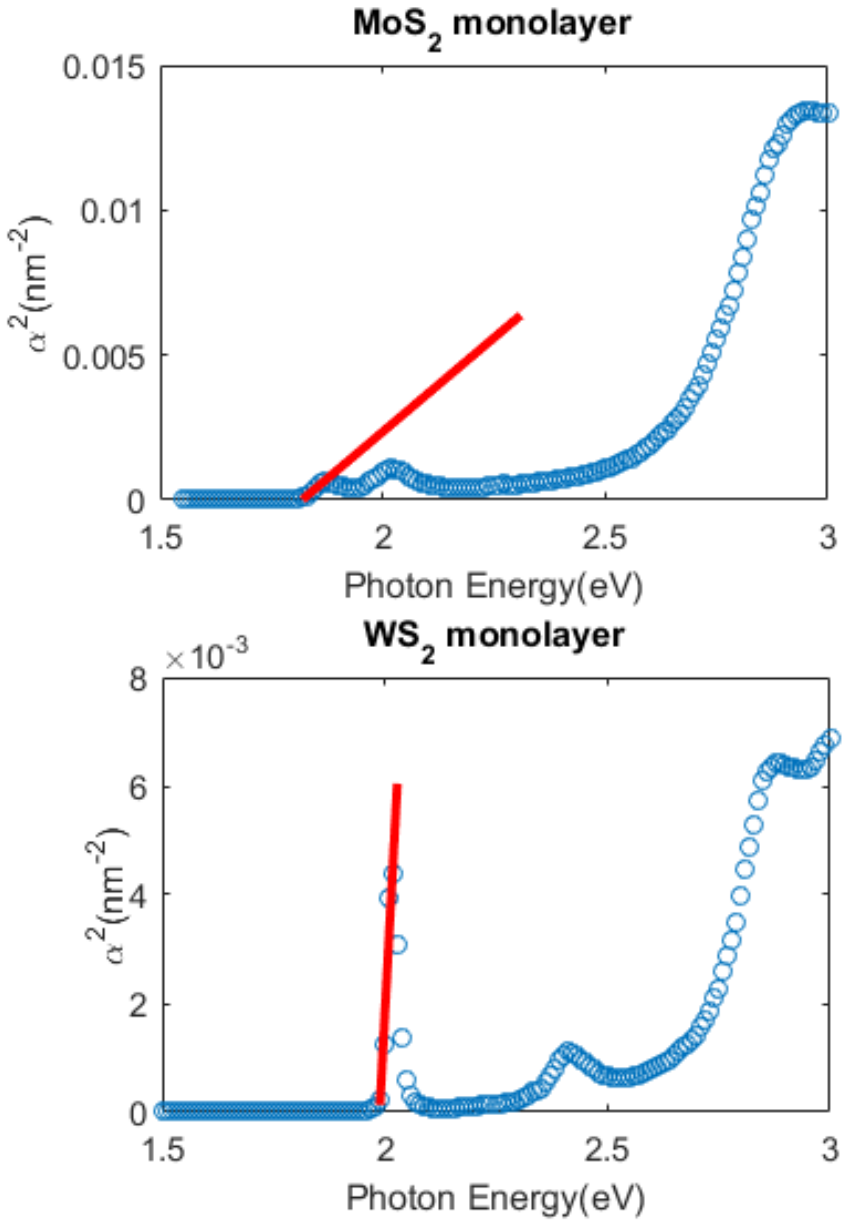

Figure 4.5 Square of the absorption versus energy for monolayer MoS_2 and WS_2; the red line is the extrapolating straight line.

The analysis for bulk MoS_2 and WS_2 is not available due to the limited range of photon energy considered in this study; the band gap energy for bulk TMDCs, shown in the previous part of the paper, is obviously much smaller than 1.50 eV, which is the minimum of the photon energy range considered in this study.

4.2 Optical Properties of MoS_2 and WS_2 on Selected Substrates

Optical properties of monolayer and bulk TMDCs on gold, silicon and fused silica wafer, as substrates, are simulated in this study. These simulations were performed in order to study the variation in the optical properties of TMDCs on a representative semiconductor, metal and insulator substrates which could contribute to understand and promote the applications of this multilayer system in areas such as coatings, electronics, optoelectronics, sensors, circuits and systems.

4.2.1 Simulation Method

In order to simulate the optical properties of the double layer, the complex dielectric constants of the substrates are needed.

Once the optical properties of the substrates are obtained, the reflectance, transmittance and absorptance can be performed by the following equations:

$$R = \frac{(n1 - n2)^2 + k1^2}{(n1 + n2)^2 + k2^2} \tag{4.12}$$

$$\alpha 1 = \frac{4\pi k1}{\lambda} \tag{4.13}$$

$$\alpha 2 = \frac{4\pi k2}{\lambda} \tag{4.14}$$

$$T = (1 - R) \times e^{-\alpha 1 t1} \times e^{-\alpha 2 t2} \tag{4.15}$$

$$A = 1 - R - T \tag{4.16}$$

The n1 and k1 are the optical constants of the upper layer, n2 and k2 are the optical constants of the substrate. α1 and α2 are the absorption coefficients of the upper layer and substrate, respectively. t1 and t2 are the thickness of the upper layer and substrate, respectively. R, T and A are the reflectance, transmittance and absorptance of the double layer structure.

4.2.2 MoS_2 and WS_2 on Gold Substrate

The thickness of the gold layer is chosen as 10μm. As mentioned in Section 4.1.3, the thicknesses of the monolayers are chosen as 0.65nm and the thicknesses of the bulk are chosen as 20nm.

Figure 4.6 represents the simulated reflectance and absorptance spectra of monolayer and bulk MoS_2 and WS_2 on gold substrate. The transmittance in the selected energy range is almost zero and thus is not presented. This is due to the opaqueness of the gold substrate.

It is observed that the reflectance tends to decrease with increase in photon energy, while the absorptance of MoS_2 and WS_2 on gold substrate increases with the increase in photon energy. The reflectance and absorptance spectra are complementary to each other due to the zero absorptance. We also observe that the change in the number of layers of MoS_2 and WS_2 does not necessarily cause a significant change in the reflectance and absorptance spectra. No sharp peaks were observed in both the spectra. Maximum values of reflectance and transmittance for monolayer and bulk MoS_2 and WS_2 on gold substrate

remained approximately the same, with an average maximum reflectance of ~90% and average maximum absorptance of ~70%.

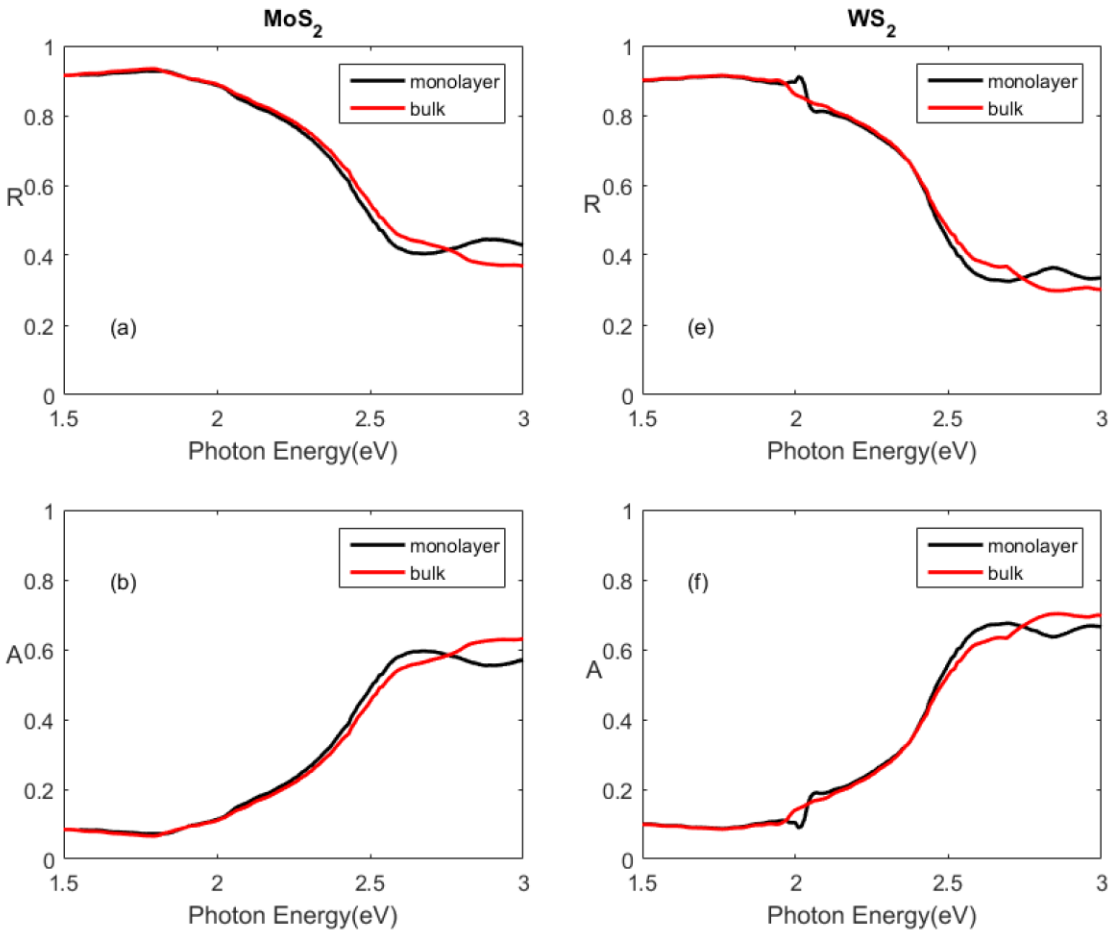

Figure 4.6 Simulated reflectance and absorptance spectra of monolayer and bulk MoS_2 and WS_2 on gold substrate.

4.2.3 MoS_2 and WS_2 on Silicon Substrate

The thickness of the silicon layer is chosen as 650mm. The thicknesses of the monolayers are chosen as 0.65nm and the thicknesses of the bulk are chosen as 20nm.

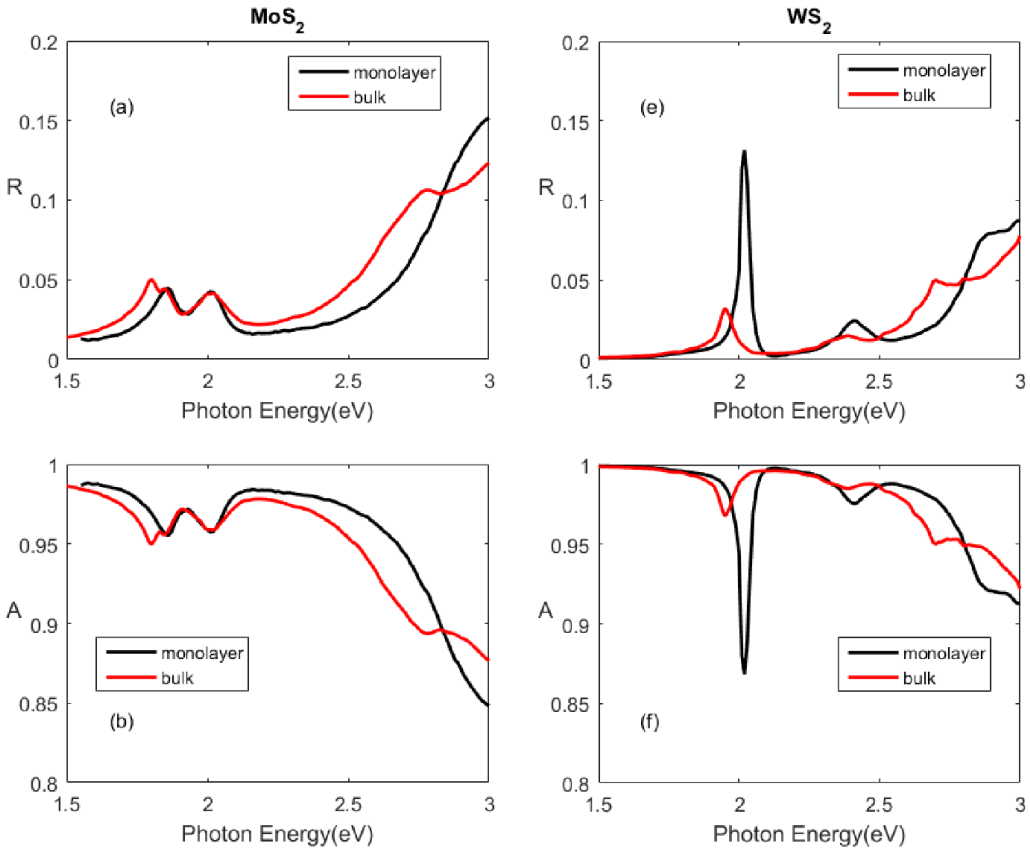

Figure 4.7 Simulated reflectance and absorptance spectra of monolayer and bulk MoS_2 and WS_2 on silicon substrate.

The transmittance in the selected energy range is almost zero due to the opaqueness of the silicon substrate. The reflectance has a relatively low value as compared to that of the gold substrate (average maximum value of ~90%). However, it is observed that there is a sharp peak in the reflectance spectra of monolayer WS_2 on silicon substrate. The absorptance of the monolayer and bulk MoS_2 and WS_2 on silicon substrate is relatively high compared to that of gold substrate.

4.2.3 MoS_2 and WS_2 on Fused Silica Substrate

The thickness of the fused silica layer is chosen as 650mm. The thicknesses of the monolayers are chosen as 0.65nm and the thicknesses of the bulk are chosen as 20nm.

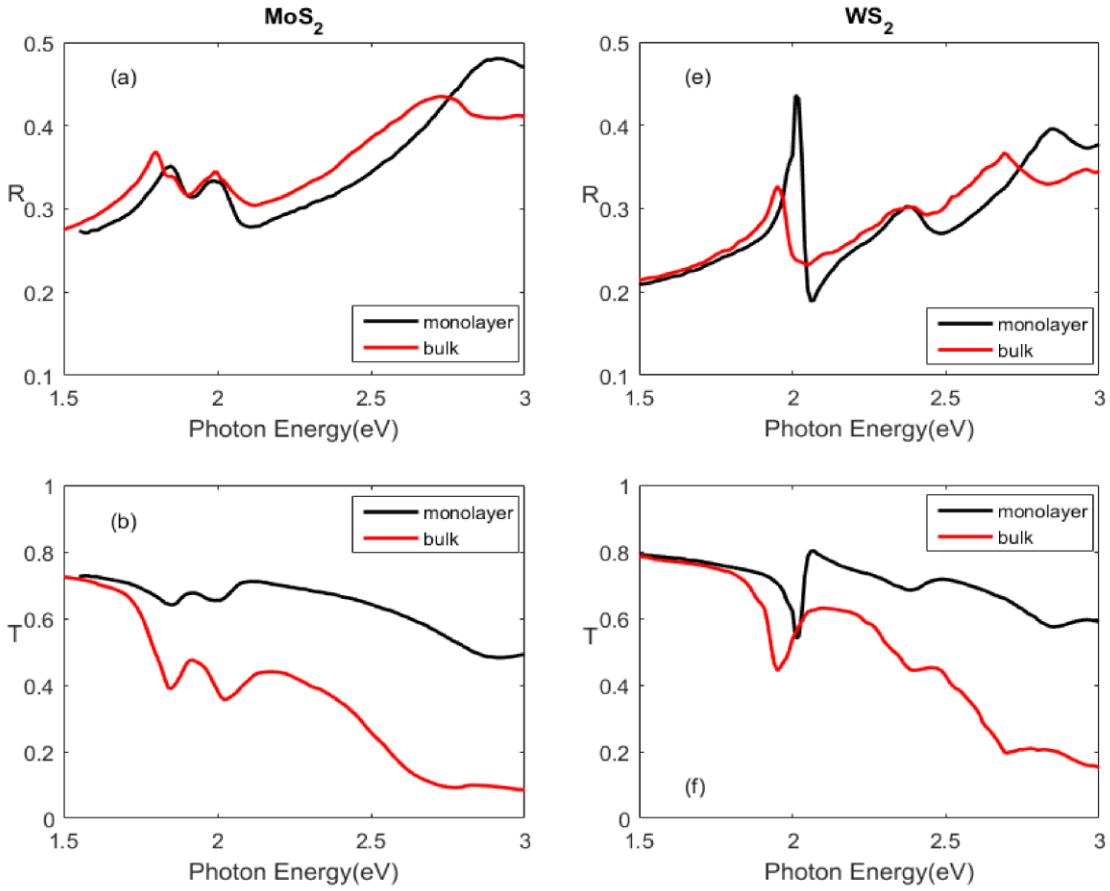

Figure 4.8 Simulated reflectance and transmittance spectra of monolayer and bulk MoS_2 and WS_2 on fused silica substrate.

Figure 4.8 presents the simulated reflectance and transmittance spectra of monolayer and bulk MoS_2 and WS_2 on fused silica substrate. It is observed that the transmittance of TMDC/fused silica is considerably high which is due to the transparent nature of fused silica and TMDCs.

As observed in Figure 4.8, the maximum value of Reflectance (R) for monolayer MoS_2 and WS_2 are 48.06% and 43.59%, respectively. Similarly, the maximum value of R for bulk MoS_2 and WS_2 are 43.48% and 34.70%, respectively.

The maximum value of Transmittance (T) for monolayer MoS_2 and WS_2 are 72.56% and 80.26%, respectively. Similarly, the maximum value of T for bulk MoS_2 and WS_2 are 72.48% and 78.64%, respectively.

Figure 4.9 presents the simulated absorptance spectra of monolayer and bulk MoS_2 and WS_2 on fused silica substrate. The maximum value of Absorptance (A) for monolayer MoS_2 and WS_2 are as follows: 3.83% and 3.26%, respectively. Similarly, the maximum value of A for bulk MoS_2 and WS_2 are 50.33% and 50.40%, respectively.

The absorptance spectra, shown in Figure 4.9, are very similar to that in Figure 4.4; however, the values differ from each other by a small factor. The trend in the change in the value of the monolayer and bulk TMDCs are the same.

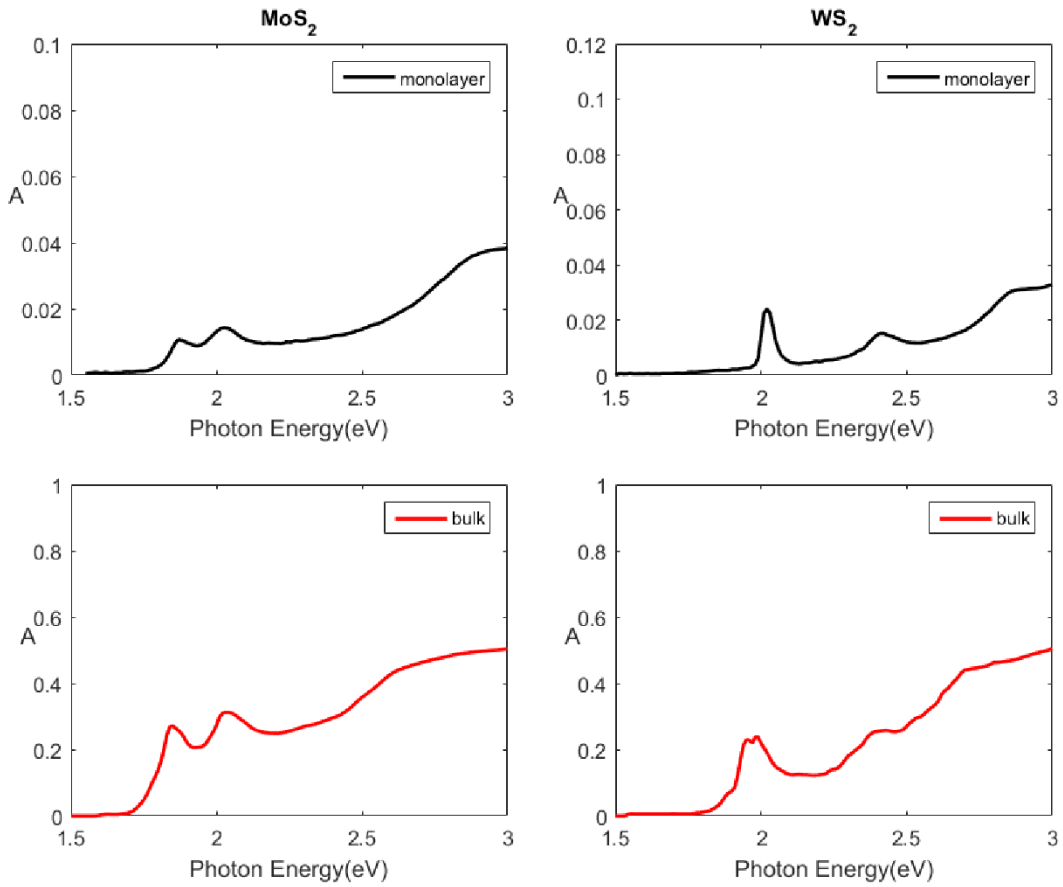

Figure 4.9 Simulated absorptance spectra of monolayer and bulk MoS_2 and WS_2 on fused silica substrate.

CHAPTER 5

APPLICATIONS OF MoS_2 and WS_2

The advances in fabrication methods such as exfoliation and synthetic techniques have made it possible to fabricate the ultra-thin monolayer TMDCs, like MoS_2 and WS_2. These two materials can be classified as semiconductors with stability in air. Their direct band gap in the visible energy range makes these materials promising in digital electronics and optoelectronics. There have been already many reports about the applications of these materials, such as Field Effect Transistors (FETs), solar cells, photodetectors etc. In this chapter, a brief overview of these applications, the architecture, operating principle and physics of electronic and optoelectronic devices will be presented.

5.1 Digital Electronics

MoS_2 and WS_2 are promising for applications in future digital electronics such as FETs, inverters, logic gates, junctions and heterostructures.

5.1.1 FET

The structures and functions of FET have already been discussed in Chapter 2. These materials have first been used in FETs only over the past decade[35]. Initially, the field-effect mobility of monolayer MoS_2 was found to be a lot lower than that in graphene[15]. However, in 2011, B. Radisavljevic et. al. have reported a monolayer MoS_2 top-gated with a relatively high mobility, large on/off ratios and low sub-threshold swings at room

temperature[11]. These reports have inspired interest for further studies. The large band gap (>1eV) and ultra-thin top gate makes it possible to achieve small cut-off currents and large switching ratios.

The recent studies focus on the difference in the mobility measured by experimental studies and the mobility by theoretically predictions. Theoretical studies now predict that the intrinsic mobility at room temperature in monolayer MoS_2 is 300-400 cm^2/Vs at high carrier densities of $10^{13}/cm^2$[18]. This value is five times greater than the largest experimentally reported values at 300K[36].

The sensitivity of carrier mobility to the local dielectric environment has inspired the studies on the electron transition mechanism. The studies in this field were carried out by temperature dependent mobility measurements. With the improvement in the sample quality and device processing, it is observed that phonon scattering is dominant for T > 100K and charged impurity scattering is dominant for T <100 K[17, 36, 37]. As for theoretical predictions, the influence of remote interfacial phonons from the oxide dielectric are considered recently, and the results show a better agreement with experimental studies[38]. The lack of considering defects and impurities also lead to overestimating the mobility values.

The contact resistance also plays an important role in determining the conductance of the FET devices. Since MoS_2 and WS_2 are ultra-thin 2-D materials, the substrates significantly influence the performance of the corresponding devices. Theoretical prediction and experimental studies on contact resistance have also been carried out [39-42]. Generally, these studies found that low work function metals such as Ti and Sc form lower resistance contacts than high work function metals which leads to higher drain

currents[39]. Nevertheless, even with the optimal contacting scheme, the contact resistance still dominates the charge transport with reduced channel dimensions.

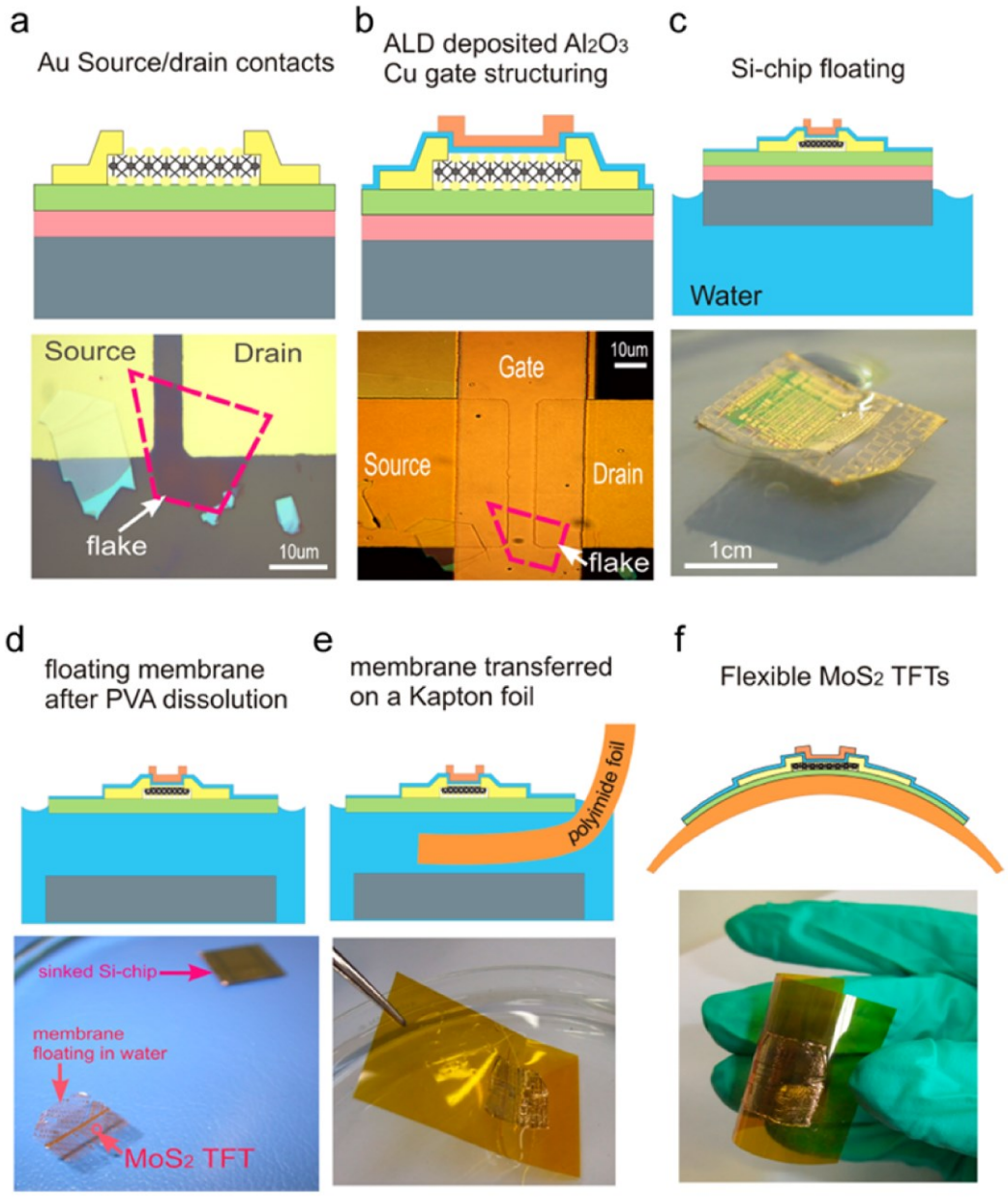

Figure 5.1 Illustration of the fabrication of flexible FET [43].

It should also be noted that these flexible 2-D materials make it possible to fabricate flexible FET on flexible substrates[44]. The influence of strain on the properties of these

materials have also been carried out[45]. Figure 5.1 presents an illustration of the fabrication of flexible FET. These initial studies demonstrate that ultra-thin FETs on flexible substrates remain a desirable parameter under mechanical bending[43, 46].

The promise of MoS_2 and WS_2 based high performance FET has inspired researchers to perform further studies on their applications to more complex, functional digital circuity inverters and logic gates[47].

5.1.2 Junctions and Heterostructures.

In addition to semiconducting TMDC based devices and circuits, these materials present possibilities for special device geometries based junctions and heterostructures [48, 49]. Such heterojunction devices have been widely developed for crystalline III-V semiconductors for high frequency applications.

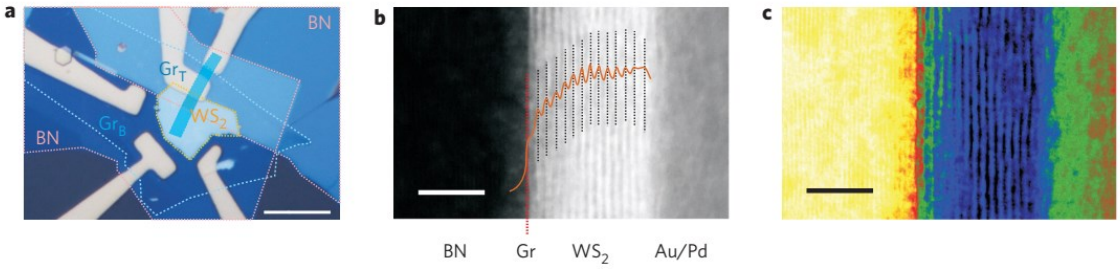

Figure 5.2 Illustration of Graphene–WS_2 heterotransistor. a) Optical image (scale bar, 10 mm). b) Cross-section high-resolution high-angle annular dark-field scanning transmission electron microscopy (HAADF STEM) image (scale bar, 5 nm). c) Bright-field STEM image (scale bar, 5 nm) [48].

Epitaxy is the most common method for the growth of III-V semiconductor heterostructures. This limits the materials to possess relatively similar lattice constants. The

weak Van der Waals bonding between TMDCs can relax this limit and thus enhance the possibilities for different materials to form different heterostructures [50].

5.2 Optoelectronics

In Chapter 3, it was shown that monolayer MoS_2 and WS_2 have direct band gap in the visible region of the electromagnetic spectrum and large binding energies. These two materials also have strong photoluminescence. These properties make them promising candidates in applications in optoelectronics including photodetectors, photovoltaics and light-emitting devices.

5.2.1 Photodetectors

When the energy of the incident photon is larger than the band gap of a semiconductor, bound electron-hole pairs (or excitons) or free carriers, which depend on the exciton binding energy in the semiconductor, are created. Bound excitons can be separated by an applied or build-in electric field and thus generate a photocurrent. The most common two types of photodetectors are phototransistors and photodiodes.

Phototransistors are types of bipolar transistors with their base lead removed and replaced with a light-sensitive area. These devices have only two terminals. When the light-sensitive area is in dark, the device is turned off. When the light-sensitive region is exposed to light, a small base current is generated that controls a much larger collector-to-emitter current.

In the initial studies, MoS_2-based phototransistors were measured under global illumination with photons possessing energies greater than the 1.9 eV band gap[51].

Recently, few-layer WS_2 phototransistors, grown by CVD, have also been reported[52]. The wavelength-dependent studies show that the photocurrent roughly follows the absorption spectrum; this has led to the speculation of inter band absorption and carrier separation as the dominant mechanism for photocurrent generation[53, 54].

A photodiode is a semiconductor device that converts light into current. The current is generated when photons are absorbed in the photodiode. A small amount of current is also produced when no light is present. It is reported that vertical Si/Monolayer MoS_2 heterostructures exhibit photodiode-like behavior and excellent photon response[55]. Similar results have also been found on vertically stacked graphene-MoS_2-metal heterostructures[56].

5.2.2 Solar Cells and Light-emitting Devices

The photovoltaic cell is one of the most widespread application of p-n junctions. Semiconductors with high mobility and direct band gap near 1.3eV is desired for high efficiency single junction photovoltaics. The monolayer TMDCs are in good agreement with the frontier needs, which makes them promising in ultra-thin photovoltaic applications.

In 2013, a calculation on a Schottky junction solar cell, consisting of a graphene-MoS_2 stack, suggests a maximum power conversion efficiency of ~1% while that of a Type-II heterojunction between WS_2/MoS_2 is 1.5%[57]. Experimentally, an asymmetric M-S-M Schottky junction on a few-layer MoS_2 flake resulted in working photovoltaic devices with ~1 % PCE in the same year[58]. Although the above results are encouraging, the thickness limited absorption is still a significant barrier to increase the efficiency.

LED, the light-emitting diode, is another promising application for MoS_2 and WS_2 p-n junctions. Their ultra-thin thickness and direct band gap with desired energy makes them promising for ultra-thin, efficient and flexible LEDs. Excitonic electroluminescence has been observed from SL-MoS_2 heterojunctions so far[59]. However, the lack of controlled doping technologies make it only possible to fabricate purely monolayers and limit their applications.

CHAPTER 6

CONCLUSIONS

In Chapter 1, the basic knowledge of MoS_2 and WS_2 was introduced. Their lattice structure and constants, different stacking sequence, thickness and other basic properties were presented.

An introduction to the electrical properties of monolayer MoS_2 and WS_2 was carried out in Chapter 2. The difference observed between the mobility measured by experimental method and first principle calculation has drawn the attention for further studies. Experimental measurements, at different temperatures, provide researchers a useful method for studying the current conduction mechanisms. Considering defects and impurities in first principle simulations also decreases the difference. Other factors such as contact method and substrate material also influence the electrical properties.

In Chapter 3, the electrical structure and the temperature dependence of the band gap of MoS_2 and WS_2 were presented. For monolayer MoS_2 and WS_2, their direct band gap with energy value in the visible electromagnetic spectrum and flexibility make them promising in many fields. The temperature dependence studies of the energy gap of monolayer TMDCs, in the range of 50 to 450 K, were also presented.

In Chapter 4, the optical properties of the optical constants and optical properties of suspended monolayer and bulk MoS_2 and WS_2 were simulated by mathematical modelling utilizing MATLAB. The results are in accord with experimental data and show an appreciable convergence. The calculated optical properties of MoS_2 and WS_2 on

semiconductor, metal and fused silica substrates were presented. Absorptance is highest (~90%) for TMDC/Si while, the transmittance is highest (~90%) for TMDC/Au. TMDC/fused silica exhibits optical properties similar to that of suspended TMDCs. The optical band gaps of the monolayers were also investigated by considering the absorption coefficient versus incident energy. The results correspond to the electrical band gap investigated in Chapter 3 with a reasonable difference.

In Chapter 5, the promising applications of monolayer MoS_2 and WS_2 were discussed. Their unique properties make them promising candidates in many applications such as FETs, Schottky barriers, heterostructures, photodetectors, solar cells, LEDs etc. Although there are still many technology problems that need to be resolved, the bright future of these materials can already be predicted.

In conclusion, a detailed study on the properties and applications of MoS_2 and WS_2 has been presented. These recently emerged 2-D materials have drawn the attention of researchers by their unique properties. It is convincing that these materials will have essential part in promoting the development of materials science.

REFERENCES

[1] T. Cao, G. Wang, W. Han, H. Ye, C. Zhu, J. Shi*, et al.*, "Valley-selective circular dichroism of monolayer molybdenum disulphide," *Nature communications,* vol. 3, p. 887, 2012.

[2] X. Wang and F. Xia, "Van der Waals heterostructures: Stacked 2D materials shed light," *Nat Mater,* vol. 14, pp. 264-265, 2015.

[3] Q. H. Wang, K. Kalantar-Zadeh, A. Kis, J. N. Coleman, and M. S. Strano, "Electronics and optoelectronics of two-dimensional transition metal dichalcogenides," *Nature nanotechnology,* vol. 7, pp. 699-712, 2012.

[4] Z. Wang, Q. Su, G. Yin, J. Shi, H. Deng, J. Guan*, et al.*, "Structure and electronic properties of transition metal dichalcogenide MX_2 (M= Mo, W, Nb; X= S, Se) monolayers with grain boundaries," *Materials Chemistry and Physics,* vol. 147, pp. 1068-1073, 2014.

[5] K. F. Mak, C. Lee, J. Hone, J. Shan, and T. F. Heinz, "Atomically thin MoS 2: a new direct-gap semiconductor," *Physical Review Letters,* vol. 105, p. 136805, 2010.

[6] H. Li, J. Wu, Z. Yin, and H. Zhang, "Preparation and applications of mechanically exfoliated single-layer and multilayer MoS_2 and WSe_2 nanosheets," *Accounts of chemical research,* vol. 47, pp. 1067-1075, 2014.

[7] B. Amin, T. P. Kaloni, and U. Schwingenschlögl, "Strain engineering of WS_2, WSe_2, and WTe_2," *RSC Advances,* vol. 4, pp. 34561-34565, 2014.

[8] B. Schönfeld, J. Huang, and S. Moss, "Anisotropic mean-square displacements (MSD) in single-crystals of 2H-and 3R-MoS_2," *Acta Crystallographica Section B: Structural Science,* vol. 39, pp. 404-407, 1983.

[9] W. M. Haynes, *CRC handbook of chemistry and physics*: CRC press, 2014.

[10] J. Wilson and A. Yoffe, "The transition metal dichalcogenides discussion and interpretation of the observed optical, electrical and structural properties," *Advances in Physics,* vol. 18, pp. 193-335, 1969.

[11] B. Radisavljevic, A. Radenovic, J. Brivio, i. V. Giacometti, and A. Kis, "Single-layer MoS_2 transistors," *Nature nanotechnology,* vol. 6, pp. 147-150, 2011.

[12] Y. Yoon, K. Ganapathi, and S. Salahuddin, "How good can monolayer MoS_2 transistors be?," *Nano letters,* vol. 11, pp. 3768-3773, 2011.

[13] W. Zhang, Z. Huang, W. Zhang, and Y. Li, "Two-dimensional semiconductors with possible high room temperature mobility," *Nano Research,* vol. 7, pp. 1731-1737, 2014.

[14] R. Fivaz and E. Mooser, "Mobility of charge carriers in semiconducting layer structures," *Physical Review,* vol. 163, p. 743, 1967.

[15] K. Novoselov, D. Jiang, F. Schedin, T. Booth, V. Khotkevich, S. Morozov*, et al.*, "Two-dimensional atomic crystals," *Proceedings of the National Academy of Sciences of the United States of America,* vol. 102, pp. 10451-10453, 2005.

[16] S. Ghatak, A. N. Pal, and A. Ghosh, "Nature of electronic states in atomically thin MoS_2 field-effect transistors," *Acs Nano,* vol. 5, pp. 7707-7712, 2011.

[17] B. Radisavljevic and A. Kis, "Mobility engineering and a metal–insulator transition in monolayer MoS_2," *Nature materials,* vol. 12, pp. 815-820, 2013.

[18] K. Kaasbjerg, K. S. Thygesen, and K. W. Jacobsen, "Phonon-limited mobility in n-type single-layer MoS_2 from first principles," *Physical Review B,* vol. 85, p. 115317, 2012.

[19] L. Liu, S. B. Kumar, Y. Ouyang, and J. Guo, "Performance limits of monolayer transition metal dichalcogenide transistors," *IEEE Transactions on Electron Devices,* vol. 58, pp. 3042-3047, 2011.

[20] S. Jo, N. Ubrig, H. Berger, A. B. Kuzmenko, and A. F. Morpurgo, "Mono-and bilayer WS_2 light-emitting transistors," *Nano letters,* vol. 14, pp. 2019-2025, 2014.

[21] D. Ovchinnikov, A. Allain, Y.-S. Huang, D. Dumcenco, and A. Kis, "Electrical transport properties of single-layer WS_2," *ACS nano,* vol. 8, pp. 8174-8181, 2014.

[22] A. Allain, J. Kang, K. Banerjee, and A. Kis, "Electrical contacts to two-dimensional semiconductors," *Nature Materials,* vol. 14, pp. 1195-1205, 2015.

[23] M. Ye, D. Winslow, D. Zhang, R. Pandey, and Y. K. Yap, "Recent advancement on the optical properties of two-dimensional molybdenum disulfide (MoS_2) thin films," *Photonics*, pp. 288-307, 2015.

[24] A. Kumar and P. Ahluwalia, "Electronic structure of transition metal dichalcogenides monolayers 1H-MX_2 (M= Mo, W; X= S, Se, Te) from ab-initio theory: new direct band gap semiconductors," *The European Physical Journal B,* vol. 85, pp. 1-7, \ 2012.

[25] B. Van Zeghbroeck, "Principles of semiconductor devices," *Colarado University,* 2004.

[26] K. O'Donnell and X. Chen, "Temperature dependence of semiconductor band gaps," *Applied Physics Letters,* vol. 58, pp. 2924-2926, 1991.

[27] S. Tongay, J. Zhou, C. Ataca, K. Lo, T. S. Matthews, J. Li*, et al.*, "Thermally driven crossover from indirect toward direct bandgap in 2D semiconductors: $MoSe_2$ versus MoS2," *Nano letters,* vol. 12, pp. 5576-5580, 2012.

[28] Z. He, Y. Sheng, Y. Rong, G.-D. Lee, J. Li, and J. H. Warner, "Layer-dependent modulation of tungsten disulfide photoluminescence by lateral electric fields," *ACS nano,* vol. 9, pp. 2740-2748, 2015.

[29] Y. Li, A. Chernikov, X. Zhang, A. Rigosi, H. M. Hill, A. M. van der Zande*, et al.*, "Measurement of the optical dielectric function of monolayer transition-metal dichalcogenides: MoS_2, $MoSe_2$, WS_2, and WSe_2," *Physical Review B,* vol. 90, p. 205422, 2014.

[30] B. Mukherjee, F. Tseng, D. Gunlycke, K. K. Amara, G. Eda, and E. Simsek, "Complex electrical permittivity of the monolayer molybdenum disulfide (MoS_2) in near UV and visible," *Optical Materials Express,* vol. 5, pp. 447-455, 2015.

[31] K. F. Mak, J. Shan, and T. F. Heinz, "Seeing many-body effects in single-and few-layer graphene: observation of two-dimensional saddle-point excitons," *Physical review letters,* vol. 106, p. 046401, 2011.

[32] A. Arora, M. Koperski, K. Nogajewski, J. Marcus, C. Faugeras, and M. Potemski, "Excitonic resonances in thin films of WSe_2: from monolayer to bulk material," *Nanoscale,* vol. 7, pp. 10421-10429, 2015.

[33] L. Mattheiss, "Band structures of transition-metal-dichalcogenide layer compounds," *Physical Review B,* vol. 8, p. 3719, 1973.

[34] A. Carvalho, R. Ribeiro, and A. C. Neto, "Band nesting and the optical response of two-dimensional semiconducting transition metal dichalcogenides," *Physical Review B,* vol. 88, p. 115205, 2013.

[35] V. Podzorov, M. Gershenson, C. Kloc, R. Zeis, and E. Bucher, "High-mobility field-effect transistors based on transition metal dichalcogenides," *Applied Physics Letters,* vol. 84, pp. 3301-3303, 2004.

[36] D. Jariwala, V. K. Sangwan, D. J. Late, J. E. Johns, V. P. Dravid, T. J. Marks*, et al.*, "Band-like transport in high mobility unencapsulated single-layer MoS_2 transistors," *Applied Physics Letters,* vol. 102, p. 173107, 2013.

[37] B. W. Baugher, H. O. Churchill, Y. Yang, and P. Jarillo-Herrero, "Intrinsic electronic transport properties of high-quality monolayer and bilayer MoS_2," *Nano letters,* vol. 13, pp. 4212-4216, 2013.

[38] L. Zeng, Z. Xin, S. Chen, G. Du, J. Kang, and X. Liu, "Remote phonon and impurity screening effect of substrate and gate dielectric on electron dynamics in single layer MoS_2," *Applied Physics Letters,* vol. 103, p. 113505, 2013.

[39] S. Das, H.-Y. Chen, A. V. Penumatcha, and J. Appenzeller, "High performance multilayer MoS_2 transistors with scandium contacts," *Nano letters,* vol. 13, pp. 100-105, 2012.

[40] I. Popov, G. Seifert, and D. Tománek, "Designing electrical contacts to MoS_2 monolayers: a computational study," *Physical review letters,* vol. 108, p. 156802, 2012.

[41] D. Liu, Y. Guo, L. Fang, and J. Robertson, "Sulfur vacancies in monolayer MoS_2 and its electrical contacts," *Applied Physics Letters,* vol. 103, p. 183113, 2013.

[42] S. Walia, S. Balendhran, Y. Wang, R. Ab Kadir, A. S. Zoolfakar, P. Atkin, *et al.*, "Characterization of metal contacts for two-dimensional MoS_2 nanoflakes," *Applied Physics Letters,* vol. 103, p. 232105, 2013.

[43] G. A. Salvatore, N. Münzenrieder, C. Barraud, L. Petti, C. Zysset, L. Büthe, *et al.*, "Fabrication and transfer of flexible few-layers MoS_2 thin film transistors to any arbitrary substrate," *ACS nano,* vol. 7, pp. 8809-8815, 2013.

[44] G.-H. Lee, Y.-J. Yu, X. Cui, N. Petrone, C.-H. Lee, M. S. Choi, *et al.*, "Flexible and transparent MoS_2 field-effect transistors on hexagonal boron nitride-graphene heterostructures," *ACS nano,* vol. 7, pp. 7931-7936, 2013.

[45] H. Shi, H. Pan, Y.-W. Zhang, and B. I. Yakobson, "Quasiparticle band structures and optical properties of strained monolayer MoS_2 and WS_2," *Physical Review B,* vol. 87, p. 155304, 2013.

[46] H.-Y. Chang, S. Yang, J. Lee, L. Tao, W.-S. Hwang, D. Jena, *et al.*, "High-performance, highly bendable MoS_2 transistors with high-k dielectrics for flexible low-power systems," *ACS nano,* vol. 7, pp. 5446-5452, 2013.

[47] H. Wang, L. Yu, Y.-H. Lee, W. Fang, A. Hsu, P. Herring, *et al.*, "Large-scale 2D electronics based on single-layer MoS_2 grown by chemical vapor deposition,"presented at 2012 IEEE International Electron Devices Meeting (IEDM), San Francisco, CA, USA, Dec. 10-13,2012.

[48] T. Georgiou, R. Jalil, B. D. Belle, L. Britnell, R. V. Gorbachev, S. V. Morozov, *et al.*, "Vertical field-effect transistor based on graphene-WS_2 heterostructures for flexible and transparent electronics," *Nature nanotechnology,* vol. 8, pp. 100-103, 2013.

[49] W. Zhang, C.-P. Chuu, J.-K. Huang, C.-H. Chen, M.-L. Tsai, Y.-H. Chang, *et al.*, "Ultrahigh-gain photodetectors based on atomically thin graphene-MoS_2 heterostructures," *Scientific reports,* vol. 4, p. 3826, 2014.

[50] A. K. Geim and I. V. Grigorieva, "Van der Waals heterostructures," *Nature,* vol. 499, pp. 419-425, 2013.

[51] W. Choi, M. Y. Cho, A. Konar, J. H. Lee, G. B. Cha, S. C. Hong, *et al.*, "High- detectivity multilayer MoS_2 phototransistors with spectral response from ultraviolet to infrared," *Advanced materials,* vol. 24, pp. 5832-5836, 2012.

[52] N. Perea- López, A. L. Elías, A. Berkdemir, A. Castro- Beltran, H. R. Gutiérrez, S. Feng, *et al.*, "Photosensor Device Based on Few- Layered WS_2 Films," *Advanced Functional Materials,* vol. 23, pp. 5511-5517, 2013.

[53] Z. Yin, H. Li, H. Li, L. Jiang, Y. Shi, Y. Sun, *et al.*, "Single-layer MoS_2 phototransistors," *ACS nano,* vol. 6, pp. 74-80, 2011.

[54] H. S. Lee, S.-W. Min, Y.-G. Chang, M. K. Park, T. Nam, H. Kim, *et al.*, "MoS_2 nanosheet phototransistors with thickness-modulated optical energy gap," *Nano letters,* vol. 12, pp. 3695-3700, 2012.

[55] Y. Li, C.-Y. Xu, J.-Y. Wang, and L. Zhen, "Photodiode-like behavior and excellent photoresponse of vertical Si/monolayer MoS_2 heterostructures," *Scientific reports,* vol. 4, 2014.

[56] S. Wi, M. Chen, H. Nam, A. C. Liu, E. Meyhofer, and X. Liang, "High blue-near ultraviolet photodiode response of vertically stacked graphene-MoS_2-metal heterostructures," *Applied Physics Letters,* vol. 104, p. 232103, 2014.

[57] M. Bernardi, M. Palummo, and J. C. Grossman, "Extraordinary sunlight absorption and one nanometer thick photovoltaics using two-dimensional monolayer materials," *Nano letters,* vol. 13, pp. 3664-3670, 2013.

[58] M. Fontana, T. Deppe, A. K. Boyd, M. Rinzan, A. Y. Liu, M. Paranjape*, et al.*, "Electron-hole transport and photovoltaic effect in gated MoS_2 Schottky junctions," *Scientific reports,* vol. 3, p. 1634, 2013.

[59] Y. Ye, Z. Ye, M. Gharghi, X. Yin, H. Zhu, M. Zhao*, et al.*, "Exciton-related electroluminescence from monolayer MoS_2," presented at the *CLEO: Science and Innovations*, San Jose, CA, USA, Jun. 8-13, 2014.

APENDIX A
MATLAB CODE

The code for the calculation of the refractive index, extinction coefficient, reflectance, transmittance and absorptance of suspended materials is as shown below:

MATLAB Code1.

```
%The original data points are captured from figure. As for each material, the inputs of the
% program are
% (1) photonenergyev1, the vector of the x values of every point (Photon Energy (eV),
% ε1);
% (2) epsilon1, the vector of the y values of every point (Photon Energy (eV), ε1);
% (3) photonenergyev2, the vector of the x values of every point (Photon Energy (eV),
% ε2);
% (4) and epsilon2, the vector of the y values of every point (Photon Energy (eV), ε2);
% (5) thickness is the value of the thickness for corresponding material.
photonenergyev1=photonenergyev1(~isnan(photonenergyev1));
photonenergyev2=photonenergyev2(~isnan(photonenergyev2));
epsilon1=epsilon1(~isnan(epsilon1));
epsilon2=epsilon2(~isnan(epsilon2));
photonenergyevfit=1.50:0.01:3;
epsilon1fit=interp1(photonenergyev1,epsilon1,photonenergyevfit,'spline');
epsilon2fit=interp1(photonenergyev2,epsilon2,photonenergyevfit,'spline');
for i=1:1:151
   p=[4 0 -4*epsilon1fit(i) 0 -epsilon2fit(i)^2];
   x=roots(p);
   for ii=1:length(x)
      if x(ii)>0 & isreal(x(ii));
         n(i)=x(ii);
         k(i)=epsilon2fit(i)/(2*n(i));
      end
```

```
    end
end
wavelength=1240./photonenergyevfit;
absorptioncoefficient=4*pi*k./wavelength;
for i=1:1:151
    R(i)=((n(i)-1)^2+k(i)^2)/...
        ((n(i)+1)^2+k(i)^2);
    T(i)=(1-R(i))*exp(-absorptioncoefficient(i)*thickness);
    A(i)=1-R(i)-T(i);
end
output=[photonenergyevfit',wavelength',n',k',R',T',A'];

% The output maxtrix is a 7*151 matrix with the following parameters,
%(1) photonenergyevfit, the vector of phtonenergy from 1.50 to 3.00;
%(2) wavelength, the vector of wavelength;
%(3) n, the vector of n;
%(4) k, the vector of k;
%(5) R, the vector of reflectance;
%(6) T, the vector of transmittance;
%(7) A, the vector of absorptance;
```

The code for the calculation of the reflectance, transmittance and absorptance of double layer structure is as shown below:

Matlab Code 2

```
% The original data points are captured from web-sources and above calculation. As for
% each double layer structure, the inputs of the program are
% (1) n1, the vector of refractive index for the upper material;
% (2) n2, the vector of refractive index for the lower material;
% (3) k1, the vector of extinction coefficient for the upper material;
% (4) k2, the vector of extinction coefficient for the lower material;
% (5) t1, the thickness of the upper material;
% (6) t2, the thickness of the lower material;
% (7)
for i=1:151;
   R(i)=((n1(i)-n2(i))^2+k1(i)^2)/...
      ((n1(i)+n2(i))^2+k1(i)^2);
   T1(i)=exp(-4*t1*pi*k1(i)/wavelength(i));
   T2(i)=exp(-4*t2*pi*k2(i)/wavelength(i));
   T(i)=(1-R(i))*T1(i)*T2(i);
   A(i)=1-R(i)-T(i);
end
output=[photonenergyevfit,wavelength,R',T',A'];

% The output maxtrix is a 7*151 matrix with the following parameters,
%(1) photonenergyevfit, the vector of phtonenergy from 1.50 to 3.00;
%(2) wavelength, the vector of wavelength;
%(3) R, the vector of reflectance;
%(4) T, the vector of transmittance;
%(5) A, the vector of absorptance;
```